# 1 First semester

## 1.1 Overview

Project involves studying CP violation of reaction

$$B^0 \to D\bar{D}K^+\pi^- \tag{1}$$

and antimatter equivalent:

$$\bar{B}^0 \to \bar{D}DK^-\pi^+. \tag{2}$$

To do so the violation could occur either in the parity aspect or charge conjugation aspect. Regarding parity violation the scalar triple product of a 4-body decay can be used, namely:

$$\begin{aligned} C_T = \vec{p}_D.(\vec{p}_K \times \vec{p}_\pi) = 0 \text{ if parity is conserved,} \\ \neq 0 \text{ if parity is violated.} \end{aligned} \tag{3}$$

In order to check for charge conjugation violation an amplitude analysis must be done which compares the number of events where $C_T > 0$ and $C_T < 0$ for both matter antimatter counterparts:

$$A_T = \frac{N(C_T > 0) - N(C_T < 0)}{N(C_T > 0) + N(C_T < 0)} \tag{4}$$

$$\bar{A}_T = \frac{N(\bar{C}_T > 0) - N(\bar{C}_T < 0)}{N(\bar{C}_T > 0) + N(\bar{C}_T < 0)} \tag{5}$$

With $A_T$ and $\bar{A}_T$ a CP violating quantity can be found which when not zero violates charge conjugation:

$$\mathcal{A} = \frac{1}{2}(A_T - \bar{A}_T). \tag{6}$$

(This is quite basic, note that the actual amplitude analysis may be multi-dimensional)

## 1.2 Triple product asymmetries in 4 body decays

All content in this section taken from [1].

The scalar triple product of three vectors is defined as:

$$\vec{a}.(\vec{b} \times \vec{c}) \tag{7}$$

And for kinematics of 4-body decays, this value for momenta is asymmetric under time reversal (T) transformations (or CP equivalently), specifically it is a T odd observable. This means under a T operation the triple product sign is inverted. Note this is not observable in a three momentum system due to the triple product being invariant under rotations (as two of the momenta can be aligned with the axes of rotation). For some particle $P$ decaying into four constituent particles:

$$P \to abcd, \tag{8}$$

where the four-momenta are taken in the reference frame of $P$. By grouping the particles, $ab$ and $cd$ both form intersecting planes along the line

$$\vec{p}_a + \vec{p}_b = -\vec{p}_c - \vec{p}_d \tag{9}$$

where $\vec{p}_a + \vec{p}_b$ is set to align with unit vector $\hat{z}$ i.e.

$$\frac{\vec{p}_a + \vec{p}_b}{|\vec{p}_a + \vec{p}_b|} = \hat{z}. \tag{10}$$

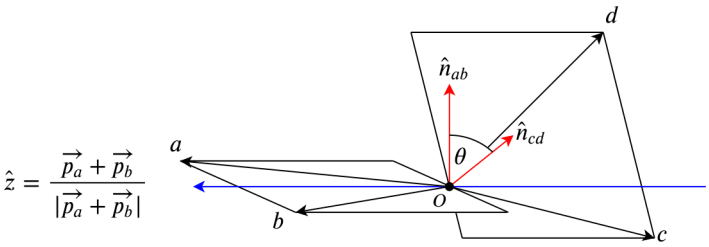


Figure 1: Shows a diagram of the decay planes and the angle between the decay planes, which is a scalar triple product.

The normal vectors of each plane are $\hat{n}_{ab}$ and $\hat{n}_{cd}$. Using these the angle between the decays plane can be found given:

$$\hat{n}_{ab}.\hat{n}_{cd} = \cos(\phi) \tag{11}$$

and

$$\hat{n}_{ab} \times \hat{n}_{cd} = \sin(\phi)\hat{z} \tag{12}$$

so using equation 12 a triple product can be formed:

$$(\hat{n}_{ab} \times \hat{n}_{cd}).\hat{z} = \sin(\phi) \tag{13}$$

so the angle intersecting the two decay planes is symmetrically odd under time reversal. Note that equation 11 is T-even i.e. is symmetrically even under time reversal because the dot product quantity is an even quantity under this transformation. Thus another T-odd quantity to measure is:

$$2(\hat{n}_{ab}.\hat{n}_{cd})(\hat{n}_{ab} \times \hat{n}_{cd}).\hat{z} = \sin(2\phi) \tag{14}$$

which can be derived from the sine double angle formula. And so using amplitude analysis of the form given in equations 6, 4 and 6 the asymmetry of equations 13 or 14 can be studied i.e.

$$A_T = \frac{N(\sin(2\phi) > 0) - N(\sin(2\phi) < 0)}{N(\sin(2\phi) > 0) + N(\sin(2\phi) < 0)}. \tag{15}$$

And so by studying the kinematics of multiple decays you can attempt to find the asymmetry and the same cane be done for the CP conjugate. Note that the triple product asymmetry is not guaranteed for a four particle system and is always vanishes in the case where two of the four products are **kinematically identical**. If this is the case the two particles are indistinguishable so when analysing the four momenta triple product the value is identical to it's antisymmetric counterpart. In the case of the angle $\phi$ this occurs in the expectation value of $\sin(\phi)$ equal to zero because by having two of the four particles being indistinguishable the momentum distribution function relative to those particles is even and so $\langle \sin(\phi) \rangle = 0$. For a more complete proof of the former, see section 2 of the reference.

The exception to this if the two particles form a resonance but then the triple product asymmetry also is dependant on the polarization of the meson states. An example reaction is:

$$B^0 \to K^{*0}(\to K^+\pi^-)\phi(\to K^+K^-) \tag{16}$$

Using the following triple product relation, asymmetry variables such as $A_T$, $\bar{A}_T$ can be defined. By studying the triple product of the momenta of three of the particles in the rest frame of $P$, define $C_T = \vec{p}_a.(\vec{p}_b \times \vec{p}_c)$ where $a$, $b$ and $c$ ar arbitrarily chosen. With this the asymmetry variables are defined as:

$$A_T = \frac{\Gamma(C_T > 0) - \Gamma(C_T < 0)}{\Gamma(C_T > 0) + \Gamma(C_T < 0)} \tag{17}$$

and

$$\bar{A}_T = \frac{\Gamma(-\bar{C}_T > 0) - \Gamma(-\bar{C}_T < 0)}{\Gamma(-\bar{C}_T > 0) + \Gamma(-\bar{C}_T < 0)} \tag{18}$$

where decays widths are compared to allow studies of asymmetries in either CP violating phases or strong phases. As before to detect any CP violation equation 6 is used and there are two cases where the value is non zero. The first case is if denominators of equations 17 and 18 are not equal which implies an asymmetry in the partial decay widths themselves. The second case is if the denominators are equal which implies that the numerators are not equal. This shows a different asymmetry which is a CP asymmetry in the triple products. In addition the average triple product asymmetry can be calculated:

$$\Sigma_T = \frac{1}{2}(A_T + \bar{A}_T), \tag{19}$$

which is not CP violating i.e. is a T-odd quantity. This is more useful for extracting information about any final state interactions which may occur as noise in the phase space analysis.

### 1.3 $\hat{C}$, $\hat{P}$ and $\hat{T}$ symmetry

In particle physics symmetries often lead to conserved quantities and in addition by violating symmetries in particle kinematics or reactions new physics can be discovered by studying reaction suppression. In particle physics three main symmetries which are often tested to validate the Standard model are parity, charge conjugation and time reversal. Parity symmetry denoted by the operator $\hat{P}$, is the action of reversing the sign of physical quantities i.e:

$$x, y, z \rightarrow -x, -y, -z \tag{20}$$

and so some physical quantities are considered to be P-odd (parity-odd) or P-even where an example of P-odd is $\vec{r}$ as shown above or $\vec{p}$. An P-even quantity would be angular momentum $\vec{L}$ as shown below:

$$\vec{L} = \vec{r} \times \vec{p} \rightarrow -\vec{r} \times -\vec{p} = \vec{r} \times \vec{p} = \vec{L}. \tag{21}$$

For a particle defined by a state $|\psi\rangle$ under parity transformation:

$$\hat{P}|\psi(\vec{r})\rangle = e^{i\phi}|\psi(-\vec{r})\rangle, \tag{22}$$

the probability density $|\psi|^2$ is conserved so parity symmetry can be conserved up to a complex phase $\phi$. Note two $\hat{P}$ operations should yield the original state up to normalisation implying

$$\hat{P}^2 = \hat{I} \tag{23}$$

where $\hat{I}$ is the identity operator. For P-even $\phi = 0$ and for P-odd $phi = \pi$ for $0 \leq \phi < 2\pi$. For $\hat{P}$ or any operation to be symmetric the commutator with respect to the Hamiltonian must be zero:

$$[\hat{H}, \hat{P}] = 0. \tag{24}$$

Charge conjugation is defined by the operator $\hat{C}$ and is the action of switching the sign of any charge quantity. As a result the operator on some particle p will switch the particle with it's antiparticle pair. So for the given particle state $|p\rangle$:

$$\hat{C}|p\rangle = |p\rangle, \tag{25}$$

thus particles that are their own antiparticle are considered $\hat{C}$ eigenstates and like parity has eigenvalues of $\pm 1$. Because parity can be violated in many particle interactions the hope is $\hat{C}\hat{P}$ would be conserved in nature where the operator $\hat{C}\hat{P}$ has eigenstates of $\hat{C}$ which is not the case anymore (e.g. $K^0 \rightleftharpoons \bar{K}^0$ has been observed but violates charge conjugation).

The time reversal operator $\hat{T}$ is one which reverses the actions of the system in time so a T symmetric quantity or process is one which doesn't change by altering the sign of $t$ as a parameter (e.g. equations of motion). So T-even values are ones which a symmetric and T-odd are ones which invert the sign of the quantity, but a considered antisymmetric. And so for some particle evolving in time described in a state $|p, t\rangle$:

$$\hat{T}|p, t\rangle = |p, -t\rangle \tag{26}$$

but note that the nature of $\hat{T}$ and $\hat{C}\hat{P}$ is that they are anti-unitary and in the description of particle physics this implies a time reversed system is a charge conjugated parity flipped system if the process was observed for forwards evolving time. Thus the following statement is true:

$$\hat{C}\hat{P}\hat{T}|p, \vec{r}, t\rangle = |\bar{p}, -\vec{r}, -t\rangle = |p, \vec{r}, t\rangle \tag{27}$$

and so from equation 27 if $\hat{C}\hat{P}$ is violated then $\hat{T}$ must be violated in order for $\hat{C}\hat{P}\hat{T}$ to remain invariant which is the continuing focus of symmetry violations in the standard model of particle physics.

### 1.4 Dalitz plots

reference [2] section 13.5.1 and 6.5.4 are good reference charm dalitz plots analysis also good, more in depth. reference [3] for 4-body example

Daltiz plots is a phase space diagram which can be used to analyse various resonances that could occur by producing a distribution of various observables, depending on the number of decay products involved in the reaction. In the case of 3-body decays the phase space is 2 dimensional with axes being the invariant masses of the 2 of the decay products. In 4-body decays the parameter space involves 5 parameters being the invariant masses of two pairs of the decay product, the cosine angles of the decay products relative to the momentum direction of the initial particle and the angle between the planes made by the decay products (see section on triple product asymmetries and decays). For example in reference [3] the following reaction is studied:

$$D^0 \to K^+K^-\pi^+\pi^- \tag{28}$$

and so the 5 parameters needed to plot the phase space are $m_{K^+K^-}$, $m_{\pi^+\pi^-}$, $\cos(\theta_K^+)$, $\cos(\theta_\pi^+)$ and $\phi$ where $\phi$ is calculated via equation 13 by comparing equation 28 to 8. The phase space plotted is known as the Lorentz invariant and a single element of the n-body LIPS takes the form:

$$d\Phi_n = \frac{1}{m!}\delta^4\left(P_i - \sum_f^n p_f\right)\prod_f^n \frac{d^3p_f}{(2\pi)^3 2E_f}, \tag{29}$$

where $n$ is the number of particles in the final state, $P_i$ is the total four-momentum of the initial state, $p_f$ is the four-momenta of the final state particles, $E_f$ is the energy of the final state and $m$ is the number of identical particles in the final state. By plotting the LIPS the information can be gained on the cross section and decay lifetimes of various resonances because the values are proportional to the LIPS and Matrix elements of the reaction

$$d\sigma, d\Gamma \propto |\langle f|\hat{T}_r|i\rangle|^2 d\Phi_n, \tag{30}$$

where $\sigma$ is the cross section, $\Gamma$ is the mean decay width of resonances, $|i\rangle$ and $|f\rangle$ are the initial and final quantum states and $\hat{T}_r$ is the Dynamical function of the resonances produced. The dynamical function is one which describes the interaction involved and when operated on by the initial and final states produces the matrix elements of the particular quantum states describing the process. The dynamical function is proportional to the matrix elements $\langle f|\mathcal{M}|i\rangle$ hence why the LIPS is proportional to the cross sections and resonance lifetimes. The Dynamical functions are often represented in S-matrix formalism of scattering theory where the matrix is unitary and defined by relative phases. An example of this is to describe the dynamical function in a K-matrix formalism (same properties as S-matrix):

$$\hat{T}_r = \left(\hat{I} - \hat{K}\rho\right)^{-1}\hat{K}, \tag{31}$$

where $\rho$ is some phase factor and $\hat{K}$ is a Lorentz invariant matrix which describes the interaction. Hence the variables used in reference [3] to plot phase space are a result of LIPS for the 4 body decay. In the context of analysis Dalitz plots can be used to identify resonances for interactions and properties of the resonance can be inferred by looking at the distribution of phase space. Regarding CP violation Dalitz plots of CP conjugate decays can be compared similar to amplitude analysis where CP conserving processes will have identical distributions and CP violating process would show some deviation for a given statistical tolerance. Denoting $\mathcal{M}$ and $\bar{\mathcal{M}}$ as the CP conjugate Dalitz plots amplitudes, A CP odd quantity can be formed by integrating the difference in amplitudes over phase space:

$$\mathcal{A}_{CP} = \int\left(\frac{\mathcal{M}-\bar{\mathcal{M}}}{\mathcal{M}+\bar{\mathcal{M}}}d\Phi_n\right)\Big/\int d\Phi_n \tag{32}$$

where the form of equation 32 is similar to equation 6 which describes single amplitude CP odd quantities. Note that the phase space will not be uniform and so rather than comparing the entire phase space for CP violation segmenting the regions of phase space would be more useful as CP violation may only occur in certain decay modes. Thus, in analysis (reference [3] for example) binning regions of phase space and individually analysing the regions proves a better detection method.

## 1.5 preliminary analysis of $\sin(\phi)$

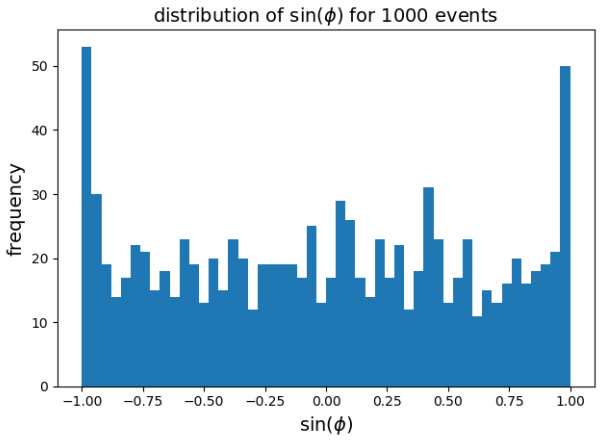


Figure 2: Shows the distribution of $\sin(\phi)$ for the 1000 generated events.

Data analysed is Monte Carlo simulated events with 1000 $B^0$ events total (equation 1). Thus, the extent of the analysis is limited to measuring equation 4 for $\sin(\phi)$ as given in equation 13, see section 1.2 for derivations and kinematics. To calculate $A_{CT}$ the number of positive and negative $\sin(\phi)$ quantities are needed so $\sin(\phi)$ is calculated for each event and then the number of positive and negative quantities are found. Figure 2 Shows the distribution of $\sin(\phi)$ and the most common angle between decay planes is $\phi = \pm\pi$ i.e. the decays most often occur along $\hat{z}$ defined by equation 10 and it was rare for all 4 particles to move perpendicular $\hat{z}$ direction. $A_{CT}$ is defined as

$$A_T = \frac{N(\sin(\phi) > 0) - N(\sin(\phi) < 0)}{N(\sin(\phi) > 0) + N(\sin(\phi) < 0)}, \tag{33}$$

and it was found that $N(\sin(\phi) > 0) = 501 \pm 22$ and $N(\sin(\phi) < 0) = 499 \pm 22$ where the error in the number of events $N$ is $\sqrt{N}$ for large N. From here $A_T$ was calculated in two ways, one by directly calculating the value and the second by Monte Carlo simulating $N(\sin(\phi) < 0)$ and $N(\sin(\phi) > 0)$. This was done by generating gaussian distributions for the variables and randomly selecting values to per Monte Carlo iteration to compute $A_T$. Then the value $A_T$ was taken as the mean value of the distribution and the uncertainty its standard deviation. This was found to converge to the same value as the error propagation method where both values give $A_T = 0.002 \pm 0.032$ which is consistent with no CP violation.

To determine the minimum asymmetry required to conclude CP violation Monte Carlo simulation is used to determine $A_T$ for varying values of $N(\sin(\phi) > 0) - N(\sin(\phi) < 0)$ and checking whether the uncertainty is smaller than the mean value. Figure 3 shows the ideal distribution to conclude some CP violation using this analysis technique. From this $A_{Tmin} > 0.05 \pm 0.03$ or $|N(\sin(\phi) > 0) - N(\sin(\phi) < 0)| > 23$ for 1000 samples. From this result it seems that to detect CP violation from $A_T$ then a larger sample is required. Alternatively a residual comparison of it's CP conjugate decay may lead to an indirect CP violation detection, as it might be the case that for the decay, $A_T$ may only be sensitive to parity. Note this does not rule out calculating $C_T = \vec{p}_a.(\vec{p}_b \times \vec{p}_c)$ though to do this the CP conjugate is required as $C_T$ alone is not CP sensitive (see section 1.4). This also requires calculating the decay width $\Gamma$ so requires software which can do a Dalitz plot analysis, which has not yet been established. Further improvements to predictions on constraints on the sample size and asymmetries is planned, and introducing confidence intervals to the analysis (other Monte Carlo simulations were attempted and this presented method agreed best with the standard error propagation method).

Other than finding the amount of asymmetry required, the number of samples needed to verify the asymmetry value can't take a value of zero (given the found asymmetry is independent of sample size)

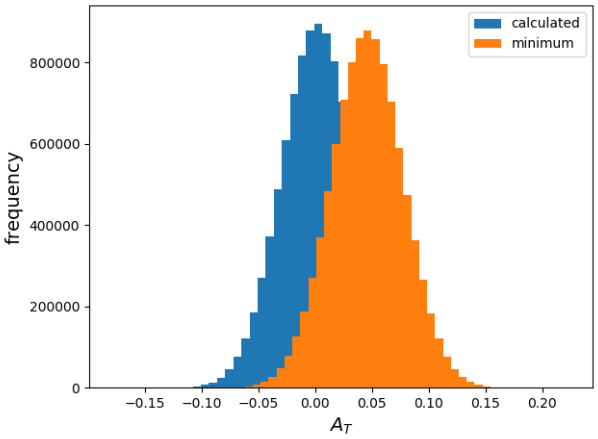


Figure 3: Shows distributions of $A_T$ where the calculated is formed by the Monte Carlo uncertainty analysis and minimum is the distribution for the minimum asymmetry required which hints towards CP violation.

can be found with the same MC simulation but rather than varying $N(\sin(\phi) > 0) - N(\sin(\phi) < 0)$, N is varied instead. To reduce the computation time a search algorithm was devised which will check if the data shows the initial hypothesis (asymmetry can't be zero). If it does not the algorithm adjusts the bounds of the sample sizes iterated i.e. if the result is null for $1000 \leq N \leq 10000$ then the bounds are adjusted to $10000 \leq N \leq 10000 * n$ for some scaling factor n. From this the minimum event number needed to find significant asymmetry is around $3 \times 10^4$ and the simulated distribution is compared to that of $A_T$ from the provided data in figure 4. Note the search is more rigorous for a smaller $n$ and that this distribution assumed that the amount of asymmetry is constant. This may not be the case and may increase with $N$ so the required samples could be less if this is the case.

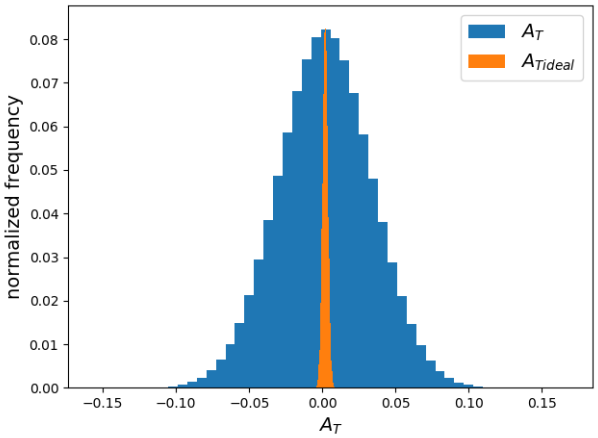


Figure 4: shows the distributions of MC simulations of $A_T$ as before and $A_{Tideal}$ which is the result of simulating the asymmetry for $N = 3 \times 10^4$, predicted by the preliminary sensitivity search. Both MC simulations are done with $10^7$ iterations and the result is for a $1\sigma$ confidence interval.

### 1.6 Phasespace Module

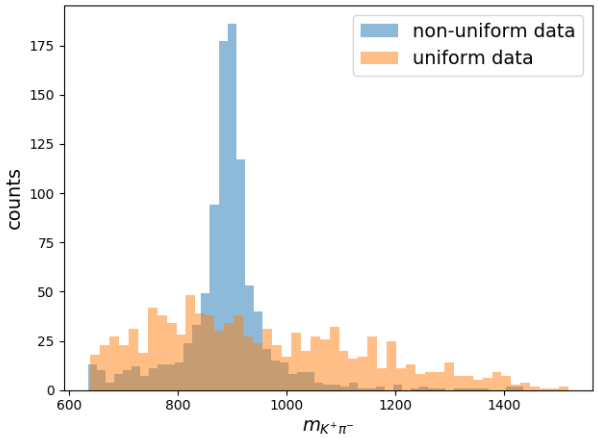


Figure 5: Shows invariant mass distributions of $K^+\pi^-$ for a non-uniform phase space (data provided) and a uniform phase space (data simulated using phasespace module). For the provided data, a clear resonance can be seen at around the mass of the particle $K^{0*}$, which decays into $K^+\pi^-$ in leading order decay processes.

To test phasespace module generates the correct events two tests have been done: first is to generate the invariant mass of the whole decay i.e.

$$s = \sqrt{P.P} = m_{B_0} \tag{34}$$

where $P = p_D + p_{\bar{D}} + p_{K^+} + p_{\pi^-}$ (sum of all decay product 4 vectors), and $P.P$ is the 4D scalar product defined as:

$$A.B = A^0B^0 - \vec{B}\vec{B} = A^0B^0 - A^1B^1 - A^2B^2 - A^3B^3 \tag{35}$$

for $A = (A^0, A^1, A^2, A^3)$ etc. As expected the phasespace generated data gives the exact result seen in 34 so the event statistics are correct. The ROOT data file has a non-uniform LIPS as the event generation considers various decay mode amplitudes and there relative weighting, calculated from Feynman diagrams and experimental results. The phasespace module doesn't take this into account but simply generates the decay events from kinematics alone, hence the LIPS is uniform. Note it may be possible to introduce resonances by also defined child decays i.e. decays after the initial $B_0$ decay which lead to the final state expected. For now the uniformity of the LIPS for a single channel decay is verified by comparing the invariant mass $m_{K^+\pi^-}$ for both the ROOT datafile and the phasespace events. The ROOT events display a resonance which comes from the the leading decay mode $K^{0*} \to K^+\pi^-$ and can be seen in figure 5. Hence a uniform LIPS will not show this feature but rather $m_{K^+\pi^-}$ will be an almost featureless distribution will less events occurring at higher energies, again shown in figure 5.

need to fit Breit Wigner distribution to resonance from ROOT file to get mass of $K^{0*}$ so phasespace can generate the child decay.

The relativistic Breit Wigner distribution is of the form:

$$f(E) = \frac{k}{(E^2 - M^2)^2 + M^2\Gamma^2} \tag{36}$$

where $k$ is equal to

$$k = \frac{2\sqrt{2}M\Gamma\gamma}{\pi\sqrt{M^2 + \gamma}}, \quad \gamma = \sqrt{M^2(M^2 + \Gamma^2)}. \tag{37}$$

Here, $E$ is the total COM energy of the resonance which has a mass $M$ and mean lifetime of $\Gamma$. $E$ can be found by computing the scalar product of the sum of 4-momenta of the child particles, so in the case of fitting the resonance in 5(blue) then $E = \sqrt{(p_{K^+} + p_{\pi^-}).(p_{K^+} + p_{\pi^-})}$.

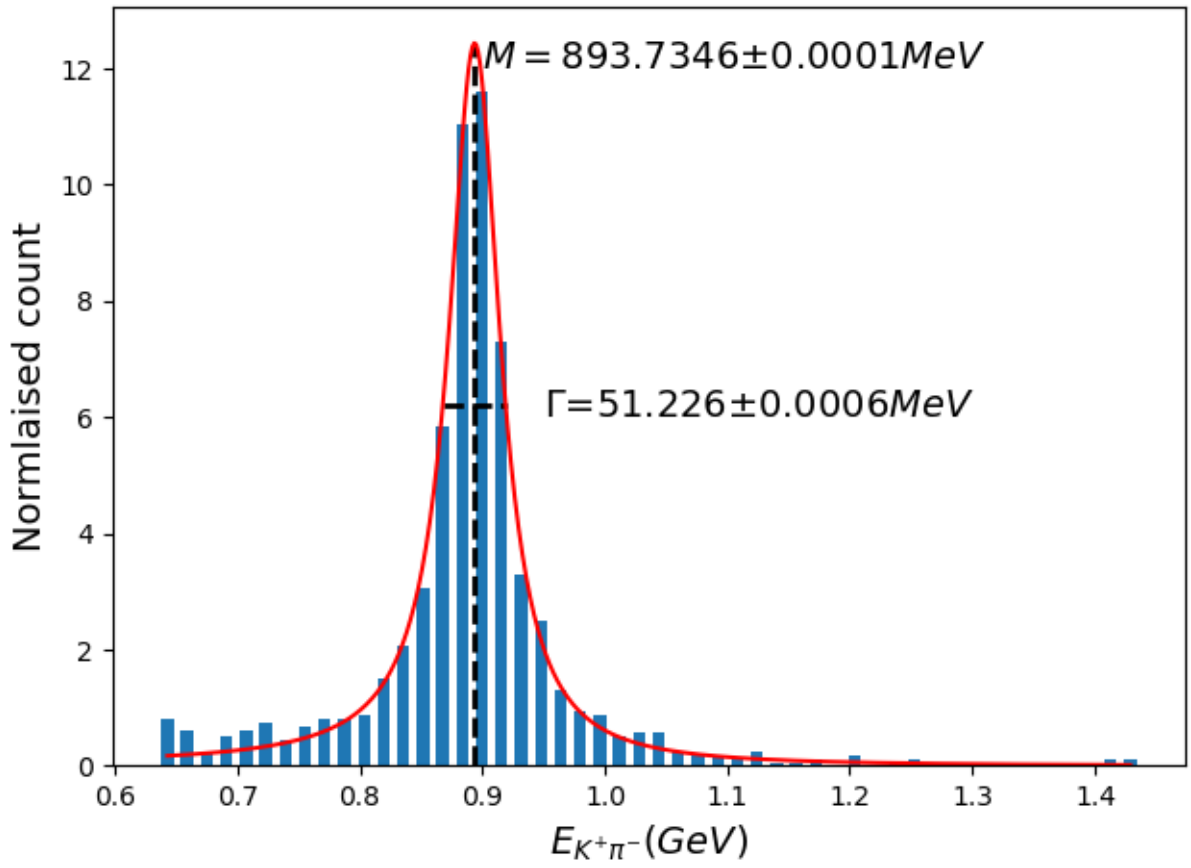


Figure 6: Shows the Distribution of $E_{k^+\pi^-}$ for the provided data with the distribution in equation 36 fitted.

the fitted curve in figure 6 was done with a least sum of squares method and gives fairly accurate values of the Mass and mean lifetime of the resonance. From this the child decay was simulated using the phasespace module using the previous method, but as before shows no distribution in the mass of the parent particle and the distribution is featureless as before. It may be possible to generate a decay and add a constraint which forces the simulation to distribute the resonance masses rather than constraining it to a single value.

Checklist:

- phasespace test for child decays. ✓
- write about sensitivity study (How it is done and what was found, possible improvements)
- look up sensitivity studies for better/ more pro method
- compute resonances for MC data and compare to phasespace data ✓
- test phasespace data i.e. does it show no CP violation ✓
- calculate $C_T$ for data ✓
- can I get confidence and sigma values in analysis?
- could I fit Breit wigner curves to invariant masses? ✓

# 2 Second Semester

## 2.1 Helicity Angle calculations

Helicity angles are $\cos(\theta_{D^0})$ and $\cos(\theta_{\pi^-})$ and are the angles the particles make with the parent particle ($B^0$) in the reference frame of the resonances $D\bar{D}$ and $K^+\pi^-$ respectively. So to find the Helicity angles do the following:

- compute resonance momentum i.e. $p_D + p_{\bar{D}}$
- define the boost matrix $B$ in terms of the 3 momentum of the resonance
- Apply the boost matrix to $B^0$ and $D$
- calculate $\cos(\theta_{D^0})$ i.e. $\frac{\vec{p_B}' . \vec{p_D}'}{|p_D'||\vec{p_B}'|}$

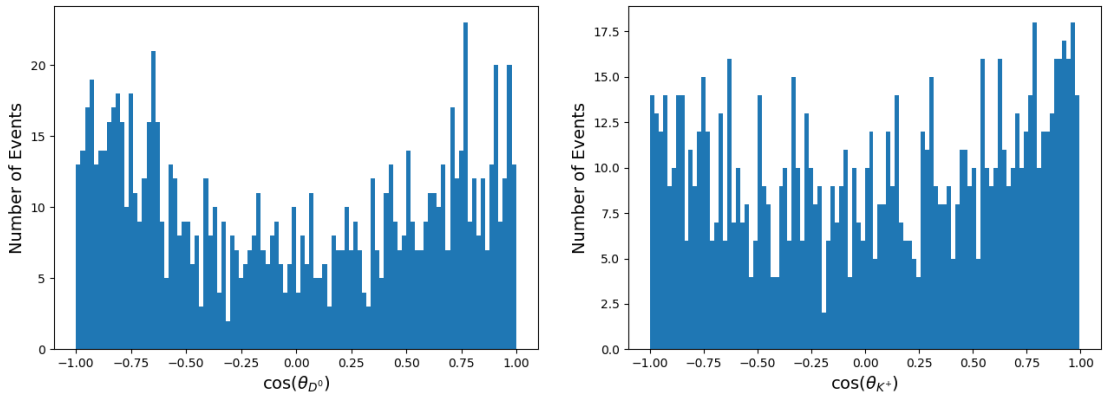


Note verification of the correct boost is done by applying the boost matrix $B$ to the frame we want to boost in (momenta should be zero). For this and other parameters, it is required to calculate these for various $C_T$ values in order to calculate $\Gamma$ for various $C_T$ values.

## 2.2 AMPGEN

.opt files contains decay channels for events where amplitudes and phases can be defined as well as constraints i.e. CP symmetry. A basic file looks like:

```
EventType D0 K+ pi- pi- pi+
#                                          Real / Amplitude    | Imaginary / Phase
#                                          Fix?  Value  Step   | Fix?  Value  Step
D0{K*(892)0{K+,pi-},rho(770)0{pi+,pi-}}    2     1      0      2     0      0
```

- `EventType` tells the generator what the ingoing and outgoing particles are. This can be set in the command line as well.
- `D0{K*(892)0{K+,pi-},rho(770)0{pi+,pi-}}` Specifies decay amplitudes for $D^0 \to K*(K^+\pi^-)\rho^0(\pi^+\pi^-)$ so you can write decay products in curly braces of the parent. The values on the right are the fix flag, real and imaginary component of the decay. When generating events, different decay channels have different weightings depending on how likely they occur i.e. $Ae^{i\phi}$. Hence, $A$ and $\phi$ is specified in the options file. For the above $A = 1$ and $\phi = 0$ as there is only one decay channel we want to consider (not accurate though), in reality there will be many channels so weightings won't be obvious. The only way to get these values is from real data analysis. The fix flag decides how the weighting should vary. If the flag is 0 it is free i.e. can change under normalisation, if it is 2 is is fixed and if it is 3 then the weighting is considered as a JIT compile time constant which won't be altered in any case including normalisation so can heavily constrain decays.

• the step size value tells you at what point should this decay be considered. The step is 0 for in both cases because the entire decay is considered in one line but, it can be split into multiple lines where the step size is added. The step must either sum to 1 or the step of a predefined decay.

It might also be that the decay can produce multiple orbital angular momentum final states. This can be added by using [] in front of the initial state:

```
a(1)(1260)+{rho(770)0,pi+}
a(1)(1260)+[D]{rho(770)0,pi+}
```

Have made and opt file of $D \to K^+K^-\pi^+\pi^-$ without small CP violation constraints. Test and see differences (might be optimisation).

### 2.3 Constructing Event files for our Decay

To create the AmpGen file, use the existing MINT file to see what resonances need to be added (apparently there might be some prebuilt ones). The idea is to add one decay amplitude and phase at a time and test if the file generates events (also do some plots to see if things work correctly).

Z(c) is not listed in the pdg.

kappa0 not listed.

D(s2)(2573)+ cant be used as spin is not defined (should be 2 I think)

psi(4160) decay event is not added to the coherent sum (is this an issue?) (tried the event on its own and it still wasn't added.)

psi(4415) not added to coherent sum.

B0psi(3770)0D0,Dbar0,kappa0K+,pi- is not recognised as a decay channel (likely because kapp0 is listed) hence not added to coherent sum. same applies for all decays with daughter of kappa0.

above applies to all daughter particles containing K(0)*(1430)0.

Potential issue is the PDG is from 2008 (ouch) so AmpGen Documentation recommends to add additional particles options/MintDalitzSpecialParticles.csv

look for PDG-MC vlaues to get particle names.

turns out psi particles are listed somewhere (not in the pdg) so the reason the coherent sum isn't added is for some other reason.

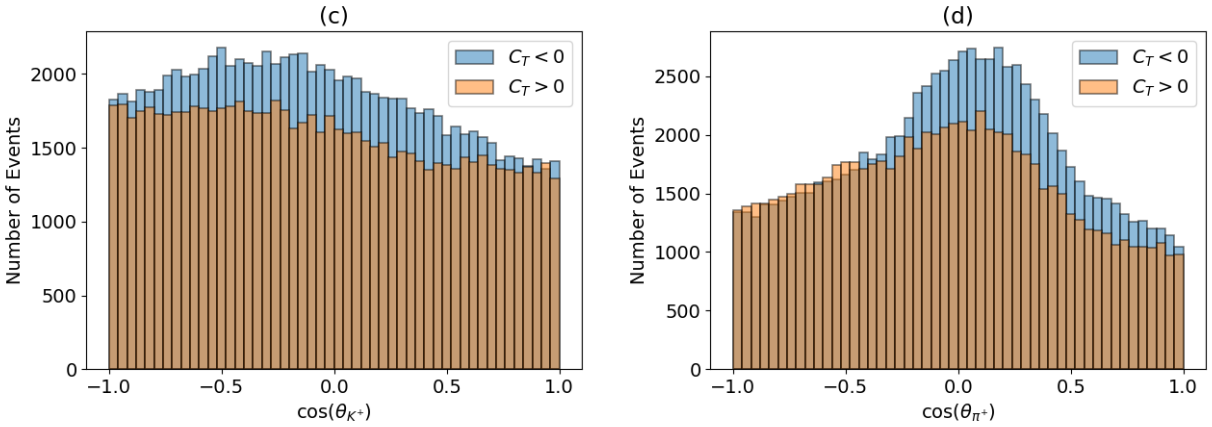


Figure 7: Shows simulated helicity angles of the decay planes for $D \to K^+K^-\pi^+\pi^-$. Number of samples used was from literature.

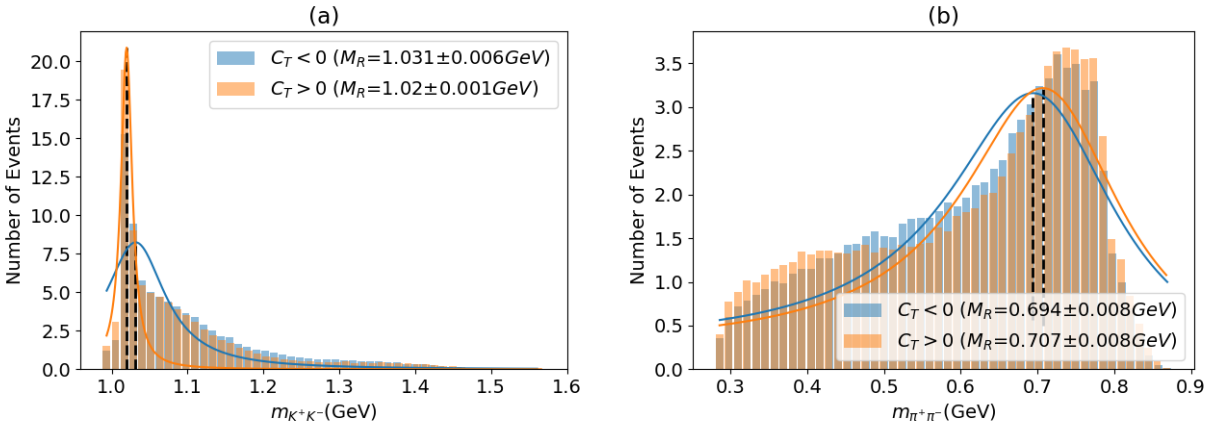


Figure 8: Shows simulated invariant mass distributions of the decay $D \to K^+K^-\pi^+\pi^-$. Number of samples used was from literature.

## 2.4 AmpGen Verification

To verify that AmpGen is working as intended, the decay $D \to K^+K^-\pi^+\pi^-$ is tested. To do so the triple product asymmetry $A_T$ was calculated for the same number of events used in the literature, and the value and statistical uncertainty will be compared. In the literature 171300 events were used. From this, $C_T$ was calculated and from this, $A_T$ as defined in equation 33 but for $C_T$ rather than $\sin(\phi)$. From this we find $A_T = -7.4 \pm 0.2\%$ for the MC toy models and the literature finds $A_T = -7.18 \pm 0.41\%$ and agrees well with the simulated data. So from this we know that AmpGen is quite accurate and should be able to replicate the $B$ decay we need to model (if the event file is correct).

CP conjugate decays using AmpGen were done simply by changing the seed of the event generator, so a different random number sequence is used and then $\bar{C}_T$ is calculated by inverting the sign of the 3-momenta of each events. From this equations 5 and 6 are calculated for 171300 events of $D \to K^+K^-\pi^+\pi^-$ and $10^5$ events for the decay in equation 30.

For the 4-body D meson decay $\mathcal{A}_{CP} = -0.07 \pm 0.34(stat)\%$.

For the 4-body $B^0$ meson decay $\mathcal{A}_{CP} = 0.17 \pm 0.45\%$.

Compared to the literature $\mathcal{A}_{CP} = 0.18 \pm 0.29(stat)\%$ for the D meson decay. This agrees with the simulation though it is interesting to note that the sign of the asymmetry is different (not to important) but

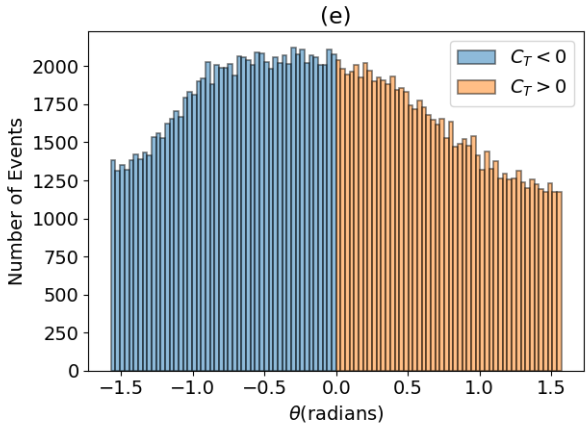


Figure 9: Shows simulated decay plane angle (scalar triple product) for $D \to K^+K^-\pi^+\pi^-$. Number of samples used was from literature.

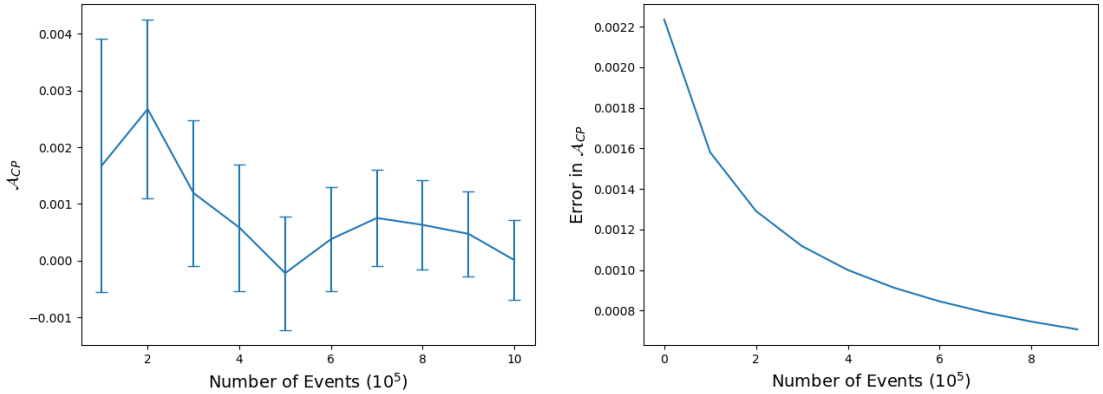


Figure 10: Left shoes the value of $\mathcal{A}_{CP}$ against the number of events. Right shows the error in $\mathcal{A}_{CP}$. Both are for $B^0$ decay.

the magnitude of the asymmetry is much smaller in the generated data though, the uncertainties are the same. This could be due to the fact generated data will contain no background signal to eliminate resulting in more precise data than in reality.

For $\mathcal{A}_{CP}$ for the $B^0$ decay, a sensitivity study was done and requires $2 \times 10^5$ events for a $1\sigma$ confidence interval and $5 \times 10^6$ for a $5\sigma$ confidence interval. To check if the asymmetry will increase with the sample size, plots of error and value of $\mathcal{A}_{CP}$ will be made for various event sizes and if the error plot and value plot cross each, other then there is a sample size for which the asymmetry can be observed, if not then that indicates the model events we are using don't show CP violation (or our C-conjugate method is wrong).

Currently trying to generate $1 \times 10^5$ to $1 \times 10^6$ events.

From figure 10 as the iteration number increases the value of the asymmetry fluctuates but gradually decreases. Also note from figure 10 the uncertainty also decreases but appears to tend towards zero implying that in this model CP violation is not present (plus error bars should be at least $3\sigma$ to be promising).

Figure 11 shows that the seed used in the generator doesn't appear to alter $\mathcal{A}_{CP}$ significantly i.e. the value fluctuates within the uncertainties of the measurements. Also, the errors in $\mathcal{A}_{CP}$ are roughly the same so the seed has no effect on this as well.

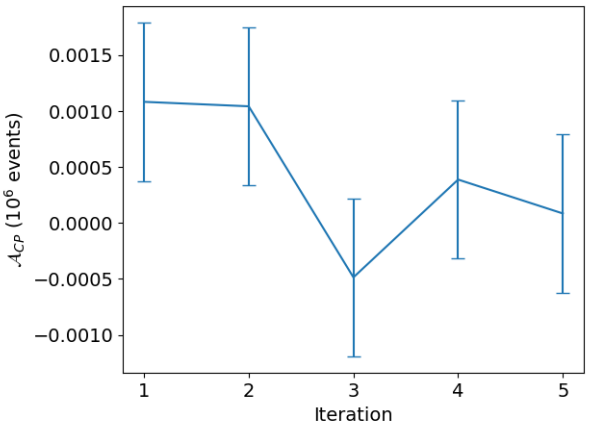


Figure 11: Shows $10^6$ events generated for $B^0$ decays, each with unique seeds.

## 2.5 Introduce Angular momentum states

Event files used up to now contain decay channels with no consideration for the various angular momentum states (s, p and d waves). In particular this effects the decay channel:

$$B^0 \to \psi(3770)(D\bar{D})K^*(892)(K^+\pi^-). \tag{38}$$

This is because the intial state is in spin 0, and the $\psi(3770)$ and $K^*(892)$ are both spin 1 particles. Hence there are 3 possible spin states the decay could end up in, shown in figure **??**.

| $B^0$ | $\psi(3770)$ | $K^*(892)$ | $\psi(3770)K^*(892)$ |
|---|---|---|---|
| 0 | 1 | -1 | 0 |
| 0 | 0 | 0 | 0 |
| 0 | -1 | 1 | 0 |

Figure 12: Shows the spin states which results in angular momentum conservation in the decay in equation 38.

For some reason, parity violation in decays is the result of interference between these S, P and D waves, particularly the P waves. Hence to Check for variations of P violation the P wave decay channels can be altered and varying amounts of P violation might be observable. For now, see how defined the s,p and d waves for reaction in equation 38 changes values (if at all). In the previous model we only consider the s-waves but now include all of them. For the new model and 10000 events $A_T = -0.022 \pm 0.003$ and the old model finds $A_T = -0.002 \pm 0.003$, so introducing the additional spin channels introduces P-violation in the system. Note also that the new model indicates P-violation up to a $7.3\sigma$ confidence interval.

To induce various levels of P violation, the amplitude for the P channel amplitudes will be increased in multiples. This will be done for 10000 events as the parity violation is significant already so is not needed to be studied in much depth.

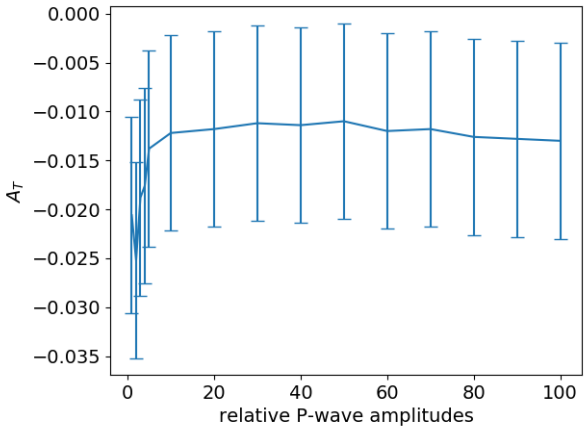


Figure 13: Shows how $A_T$ varies with the relative p-wave amplitude for the $B^0$.

Looking at figure 13 $A_T$ plateaus past a relative amplitude of 10. Note this is for each p-wave amplitude being increased so this doesn't display any property of a particular channel. Also note that the value of $A_T$ tends closer to zero as the relative amplitude increases so may do the same for $\bar{A}_T$.

For a relative amplitude of 1, a sensitivity study of $\mathcal{A}_{CP}$ was done using $1 \times 10^5$ samples and the results are shown in figure 14. From this Study, event files for the predicted samples were produced and values of $\mathcal{A}_{CP}$ were calculated shown in figure 15.

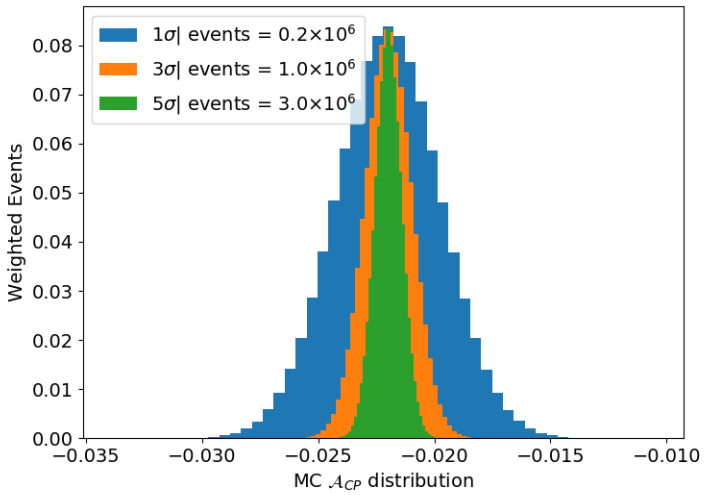


Figure 14: Shows the number of samples required to see CP violation given the amount of asymmetry seen in $1 \times 10^5$ events at various confidence intervals.

| Number of Events/Confidence interval | $2 \times 10^5/1\sigma$ | $1 \times 10^6/3\sigma$ | $3 \times 10^6/5\sigma$ |
|---|---|---|---|
| $\mathcal{A}_{CP}$ | $-0.17 \pm 0.16\%$ | $0.028 \pm 0.071\%$ | $-0.027 \pm 0.041\%$ |
| $\mathcal{A}_{CP}^{predicted}$ | $-0.21 \pm 0.16\%$ | $-0.21 \pm 0.07\%$ | $-0.21 \pm 0.04\%$ |

Figure 15: Shows the results of the sensitivity test shown in figure 14 and the values of $\mathcal{A}_{CP}$ using event files following the predictions of the study.

Looking at figure 15 the uncertainties follow the prediction well though the amount of asymmetry remains constant. This is because the sensitivity study conducted assumes a constant asymmetry present in the data which, from the table shows this value is inaccurate. The values of $\mathcal{A}_C P$ for the $3\sigma$ and $5\sigma$ intervals have a similar mean value so, for the model the amount of asymmetry present may converge to a value close to $\sim 0.0027\%$.

## 2.6 Varying P violation through SP wave interference

Now with the s,p and d waves included, varying them to see how P asymmetry varies can be done. To do this, the relative amplitudes of the p waves are adjusted by some scale factor $f$. For $f << 1$, the s wave dominates in the interference of the waves so the resulting decays will be P-even favoured and for $f >> 1$, the P-waves dominate so the resulting decays is P-odd favoured.

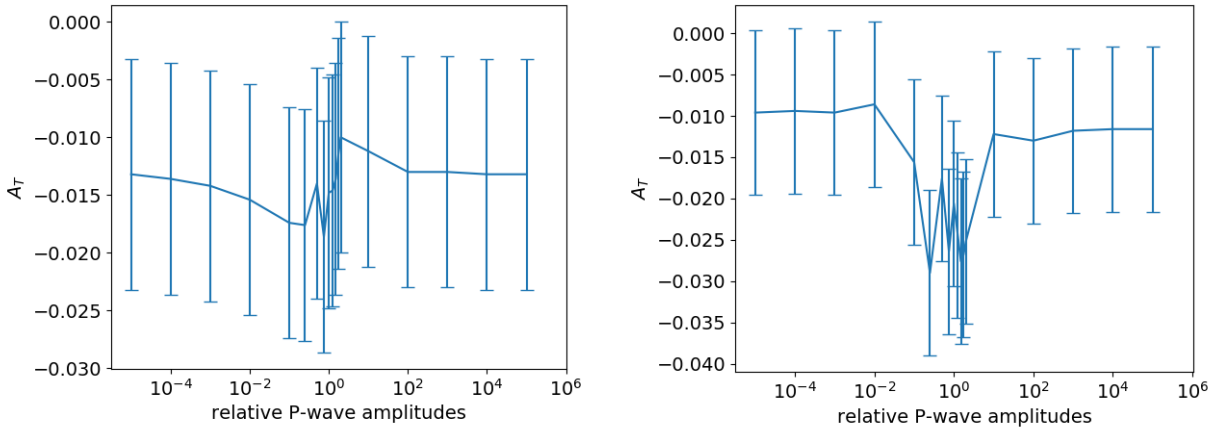


Figure 16: Left shows $A_T$ vary for the relative p wave amplitudes for the single resonance $B^0 \to \psi(3770)(D\bar{D})K^*(892)(K^+\pi^-)$. Right shows $A_T$ vary for the relative p wave amplitudes for all the currently included resonances. Both use $10^4$ events per measurement

Looking at figure 16, the values of the asymmetry doesn't go to zero when either p waves or s waves dominate the decay, for a single or multiple resonances. Close to $f = 1$, the the asymmetry maximises when all decays are considered though for $B^0 \to \psi(3770)K^*(892)$, the value is maximal for $f \simeq 0.1$ and minimal for $f \simeq 2$. Note that the initial assumption for values P-odd and P-even dominated, interference between the waves would be negligible as only one wave dominates so $A_T$ should go to zero but this is not the case for many values up to uncertainties. Possible reasons for this are additional asymmetry introduced from another source, the initial assumption was wrong, AmpGen is bugged in some way or there is an inherent bias produced from the initial state (the seed). To eliminate the bias from the seed, $10^4$ events will be constructed from 10 different seed values from which the same plot as figure 16 (right).

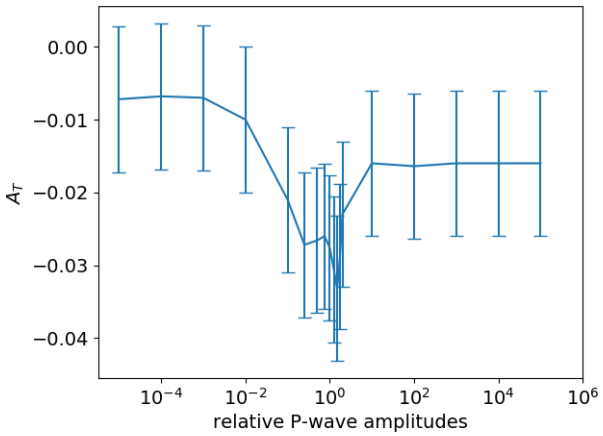


Figure 17: Shows $A_T$ vary for the relative p wave amplitudes for all the currently included resonances. Both use $10^4$ events per measurement, constructed from combining 10, $10^3$ events for different seeds (0 to 90).

From figure 17 we see that minor fluctuations in the plot are removed but do not account for the large asymmetry. A possible explantation for this offset in $A_T$ is that there is parity violation due to the phases of the p and s wave decay channels. If we consider the case of two plane waves interfering the intensity/probability of the interference is:

$$\mathcal{P} = \left| Ae^{i\phi_A(\{\Phi_n\})} + Be^{i\phi_B(\{\Phi_n\})} \right|^2 \tag{39}$$

where $A$ and $B$ are the amplitudes and $\phi_A(\{\Phi_n\})$ and $\phi_B(\{\Phi_n\})$ are the phases of the plane waves which are dependent on the LIPS defined in equation 29. Expanding equation 39 gives

$$\mathcal{P} = A^2 + AB\left(e^{i(\phi_A(\{\Phi_n\})-\phi_B(\{\Phi_n\}))} + e^{i(\phi_B(\{\Phi_n\})-\phi_A(\{\Phi_n\}))}\right) + B^2 \tag{40}$$

$$= A^2 + B^2 + 2AB\cos(\phi_A(\{\Phi_n\}) - \phi_B(\{\Phi_n\})). \tag{41}$$

Now, If we assume the P-even or P-odd limit, we can express this by assuming $A >> B$. As we are free to normalize the amplitudes, let $A = 1$ thus, $B = \epsilon$ where $\epsilon << 1$. Using these approximations equation 41 becomes:

$$\mathcal{P} = 1 + 2\epsilon\cos(\phi_A(\{\Phi_n\}) - \phi_B(\{\Phi_n\})) \tag{42}$$

$$\Rightarrow \mathcal{P} = 1 + 2\epsilon\cos(\Delta\phi(\{\Phi_n\})) \tag{43}$$

by letting $\epsilon^2 \simeq 0$ and defining the net phase $\Delta\phi(\{\Phi_n\}) = \phi_A(\{\Phi_n\}) - \phi_B(\{\Phi_n\})$. So depending on the $\Delta\phi(\Phi_n)$, $\mathcal{P}$ will change over the phase space. for $A \simeq B$ there will be some value but in the P-odd/P-even limit, the value will b close to 1. The maximal value of $\mathcal{P}$ will be $1 + 2\epsilon$ and the minimum will be one. Additional parity violation in the P-odd/P-even limit might be introduced if $\Delta\phi(\Phi_n)$ changes over the phase space for the s and p wave. The result of this is shown in equation 43 so to test for this additional source of P asymmetry, plots similar to equation 17 will be produced for different p-wave phases. The values initially will be intervals of $\frac{\pi}{2}$ To see if the $A_T$ values oscillate about zero. Unlike before, $1 \times 10^5$ events will be used to reduce the uncertainties.

BIG DETAIL MISSED IN EVENT FILES: if you want the coupling constants to be defined as the amplitude and phase the line: `CouplingConstant::Coordinates polar` must be added. Hence, for the $B^0 \to D\bar{D}K^+\pi^-$ event files we were NOT changing the amplitude but the real component of the value. However, this should not change the outcome of the result if we switch to polar coordinates up till now because all imaginary components (assumed to be phases) are zero. Hence, the coupling constants are simply real and in this case $A = x$ as $\phi = 0$ given $y = 0$.

From figure 18 the increase in event numbers reduce the uncertainties roughly by a factor of 4 but, also improves the accuracy of the plot. From this, maximal p asymmetry can be induced by setting $f = 0.5$ for all p-waves. Note that compared to figure 17 the P-even and P-odd dominated events produce asymmetries more consistent with zero, with all asymmetry uncertainties which are very large or small lying within zero. With $10^6$ events it is more likely that the values will move closer to zero. Note however, this systematic offset doesn't fluctuate around zero implying that a bias due to the seed is present. This might be due to each sample using the same set of seeds so in order to remove the systematic value of $A_T$ near the extreme regions, randomly sampled seeds for each set of events will be used.

Comparing figure 18 and 19, there is more fluctuation of the values when sampling with purely random seeds given that now at the P-odd and P-even limits, the value of $A_T$ fluctuates around zero. Note the error bars are $1\sigma$ so there my be some fluctuation outside of the uncertainty range though statistically are consistent with a zero $A_T$ value.

Now, the value of $A_T$ is compared for a varying phase and relative p-wave amplitude, testing the variability of the phase space described previously. Looking at figure 20 the value of $A_T$ for similar p wave

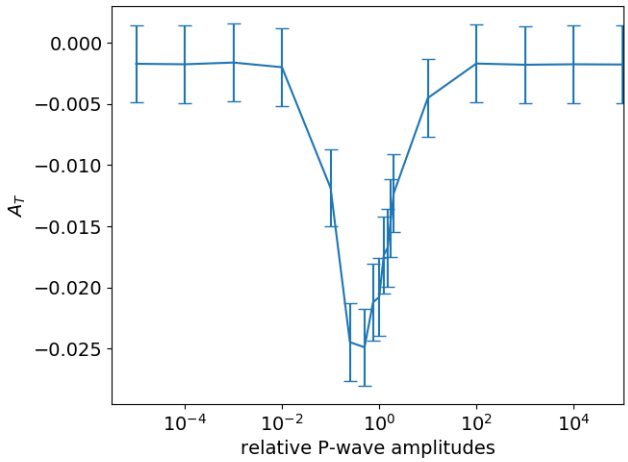


Figure 18: Shows the P asymmetry for varying p wave amplitudes, this time for $10^5$ events. Also includes multiple seeds to remove any bias due to the initial state.

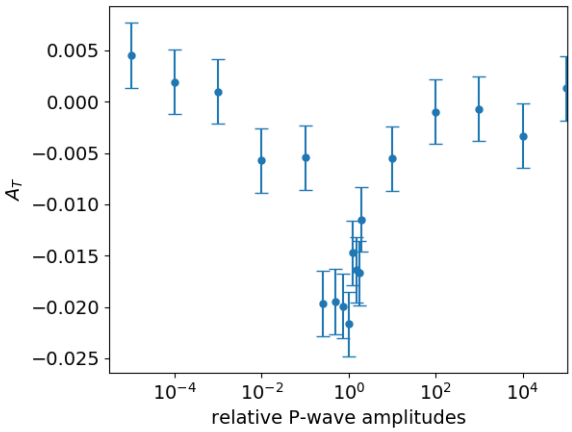


Figure 19: Shows the P asymmetry for varying p wave amplitudes for $10^5$ events using randomly generated seeds for each event file (180 in total).

and s wave amplitudes varies over the range of angles with minima and maxima at $\frac{\pi}{4}$ and $\frac{5\pi}{4}$ respectively. Naturally, the minima and maxima would be at 0 and $\pi$ respectively so the $\frac{\pi}{4}$ offset might be due to the fact the event file contain multiple resonances, and the offset is due to the sum of the remaining s-wave phases which are not varied. Despite this, The plot above can now be used to find maximal and minimal values of $A_T$ and $\bar{A}_T$ as the C conjugate decays can be constructed from the regular decay files. Hence, CP violation can be induced in the event file by using the maximum and minimum p asymmetry conditions from figure 20 i.e. set the relative p-wave phases to $\frac{\pi}{4}$ for the regular decay and $\frac{5\pi}{4}$ for the C conjugate decays.

Figure 21 shows that the CP asymmetry for varying phase and amplitude and shows no significant deviation from zero. For more events it may be possible to see a non zero $\mathcal{A}_C P$ but, from the previous sensitivity study described in figure 14 and in figure 15 it is likely that there is no significant CP asymmetry. This is due to the dependence of $\bar{A}_T$ on the phase and amplitude being similar to $A_T$ as previously mentioned.

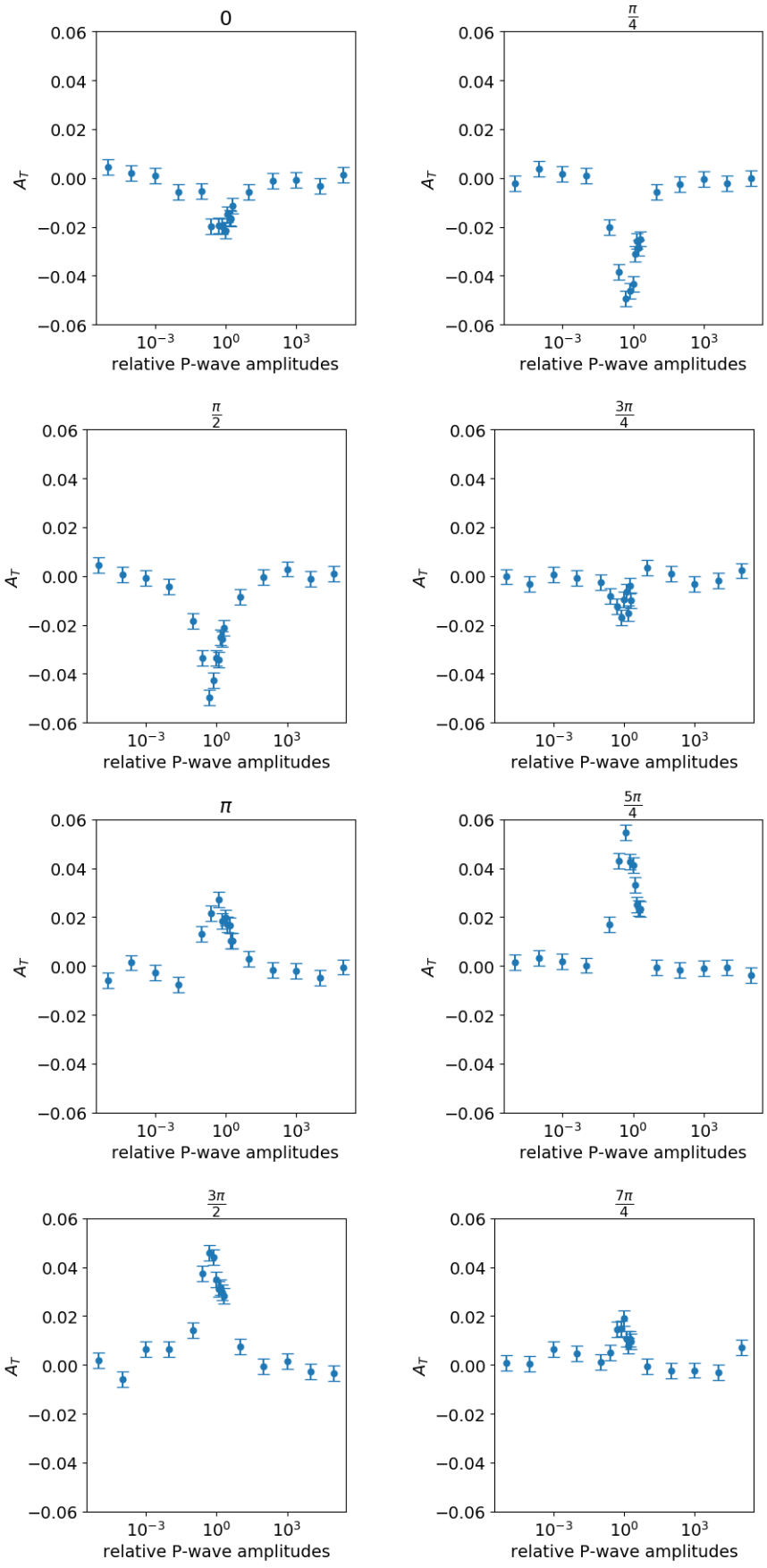


Figure 20: Shows the P asymmetry for varying p wave amplitudes and phase (shown on top) for $10^5$ events using randomly generated seeds.

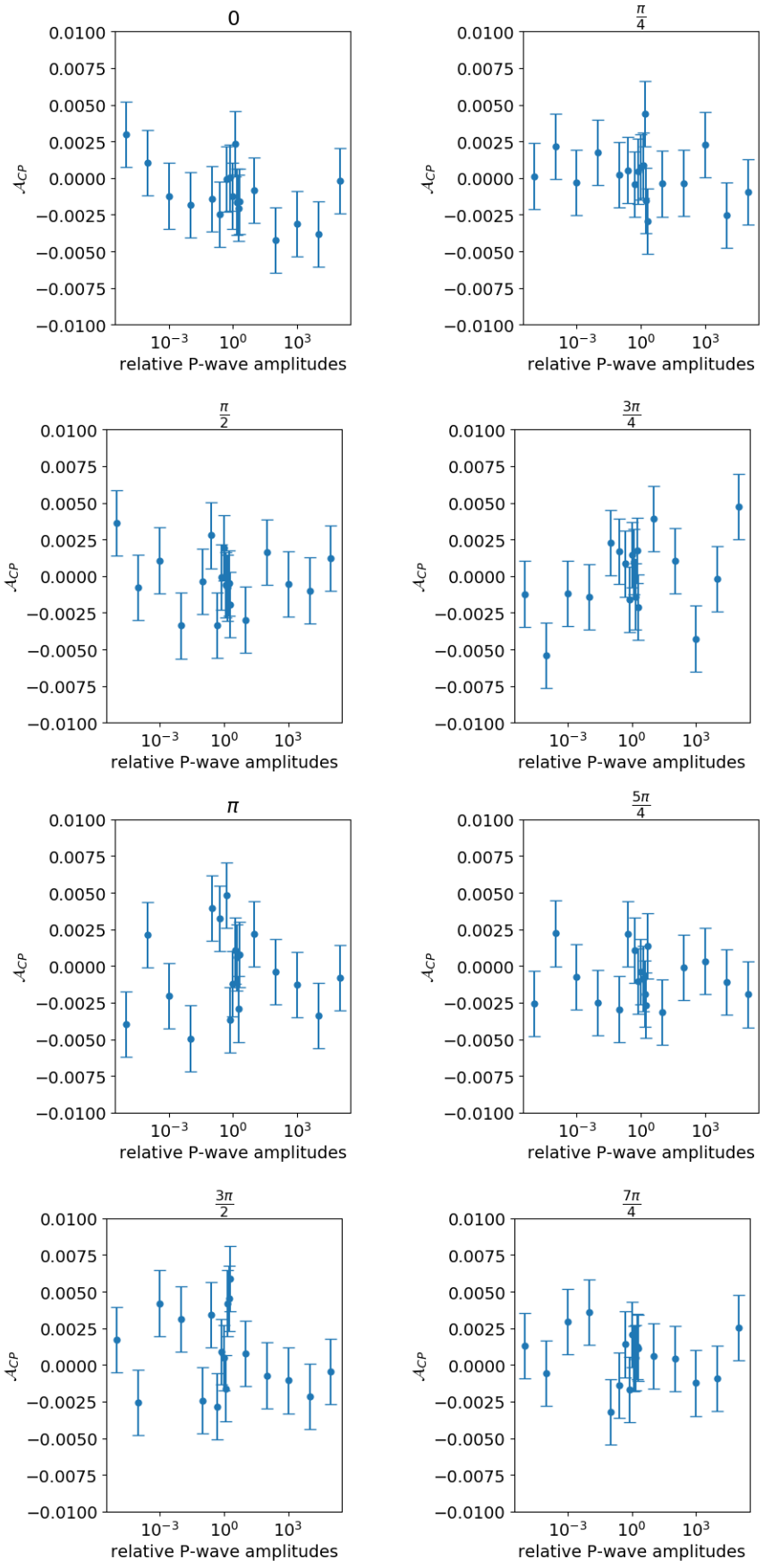


Figure 21: Shows the CP asymmetry for varying p wave amplitudes and phase (shown on top) for $10^5$ events using randomly generated seeds.

## 2.7 LHCb Data

Number of events: 2645, 1387 regular and 1258 conjugate events
Sample comes from run 1 of LHCb
The overall selection efficiency is $4.08 \times 10^{-4}$

Data from LHCb includes the 4-vectors of the decay (and many others) and includes the weights for each decay, already (how were these calculated). The weights are the ration of the signal to the background i.e.

$$w_i = \frac{S_i}{S_i + B_i} \tag{44}$$

where, $S_i$ is the number of counts corresponding to the actual signal from the decay and $B_i$ is the the number of background counts. When plotting data, weighting should be considered as the unweighted data shows both the signal and background.

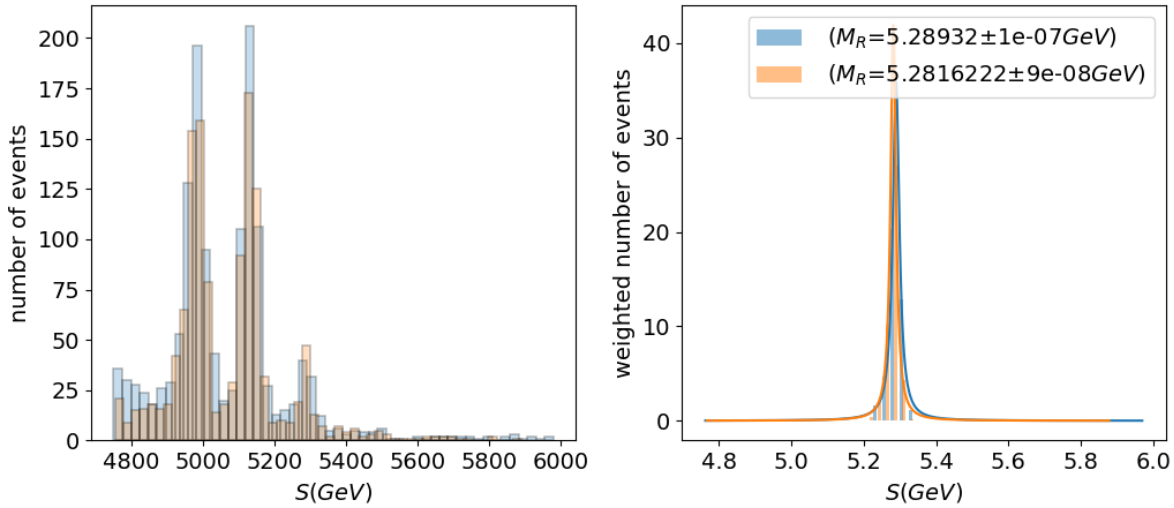


Figure 22: Right shows the distribution of the centre of mass energy $S$ without weighting the data and the left shows $S$ with the data being weighted. For the weighted data, a Breit Wigner distribution is fitted, and the resonance mass with its statistical uncertainty is displayed. The $B^0$ events are in blue and $\bar{B}^0$ are in orange.

Looking at figure 22 the data including background shows large amounts of noise and only when the the data is weighted, the expected resonance peak at around $m_{B^0}$ is clear, where the fitted value is systematically different to the current value by $\sim 9MeV$. Figure 23 shows a poorer weighting of the data (potentially) as if we compare this to figure 6, the simulated resonance peak is much clearer. A possible reason for this is the weights calculated were done considering the invariant mass of the parent particle, so the weights calculated may not apply to other quantities calculated.

When calculating $A_T$, the weighting of the data needs to be considered as the weighting of the data indicates the probability the event is the single decay we expect rather than multiple decays. Hence to find $A_T$, rather than counting the numbers of $C_T$ greater or less than zero as defined in equation 4, we need to consider the weighted distribution of $C_T$. If the weighted distribution of $C_T$ is some function $\mathcal{C}(C_T)$, then the parity asymmetry will be due to the difference in $\mathcal{C}(C_T > 0)$ and $\mathcal{C}(C_T < 0)$. As this is a continuous variable, the regions are integrated rather than counted:

$$A_T = \frac{\int_0^\infty \mathcal{C} dC_T - \int_{-\infty}^0 \mathcal{C} dC_T}{\int_{-\infty}^\infty \mathcal{C} dC_T}. \tag{45}$$

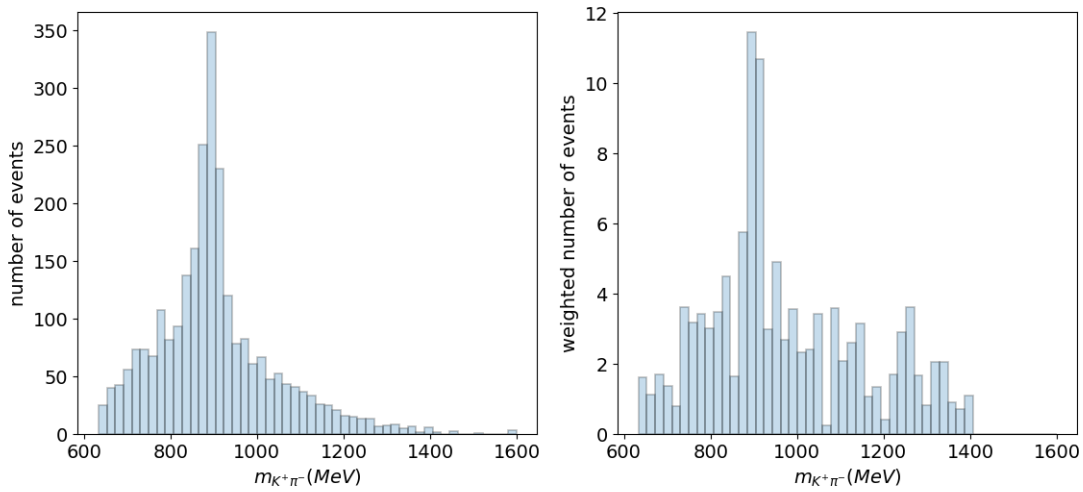


Figure 23: Right shows the distribution of $m_{K^+\pi^-}$ without weighting the data and the left shows $m_{K^+\pi^-}$ with the data being weighted.

so, equation 45 will depend on some function which needs to be fitted to the distribution and needs to be found.

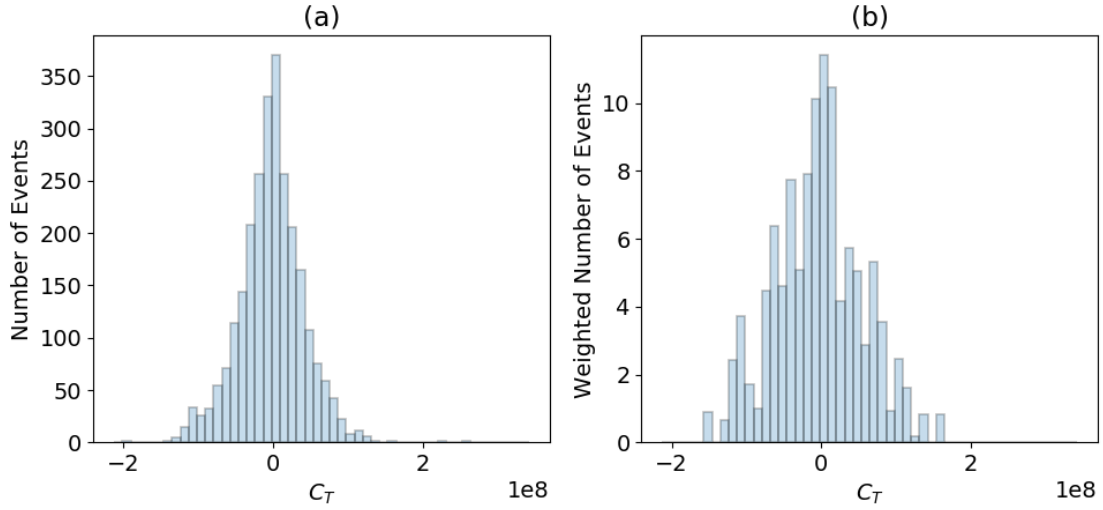


Figure 24: Figure (a) shows the distribution of $C_T$ un-weighted and Figure (b) shows the weighted distribution.

Looking at figure 24, the weighted data takes an almost Gaussian form so initially, the fit will use the Gaussian function:

$$f(x) = Ae^{-\frac{(x-B)^2}{2C^2}} \tag{46}$$

where A, B and C are free parameters to be determined by the fitting procedure.

From this approach, the asymmetry value is inconsistent with parity violation which, given the sample size is appropriate. However, note the fit value uncertainties and how low they are. From this the Gaussian fit is too weakly constrained ensuring a better fit than may be necessary. To calculate the uncertainty, the integrals in equation 45 are calculated for equation 46 except the upper and lower bounds of the fit

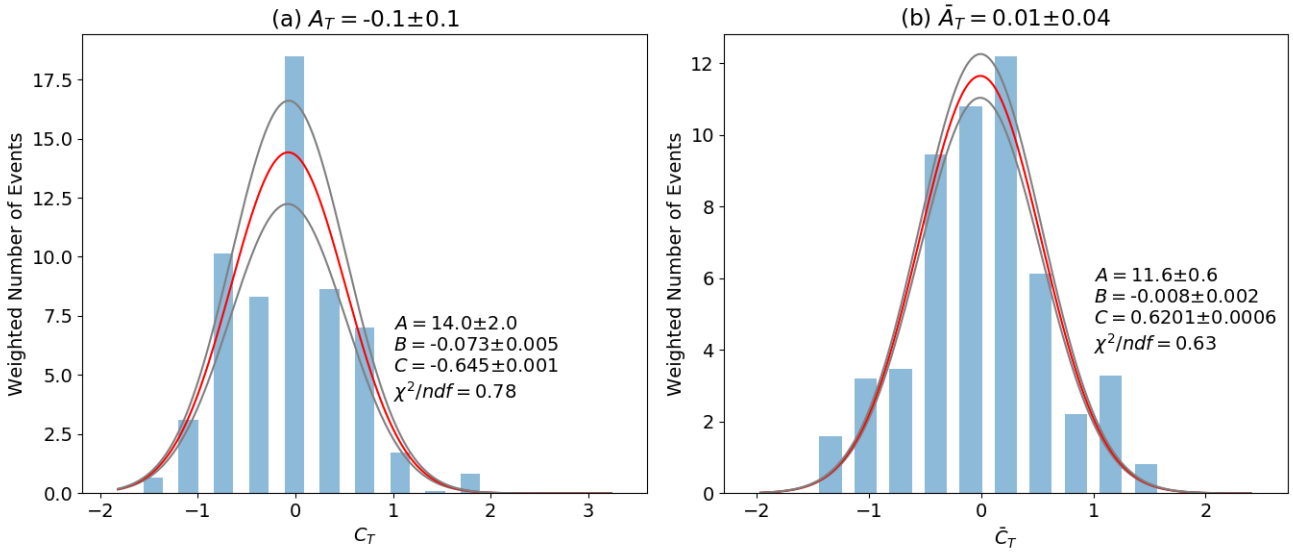


Figure 25: Figure (a) shows the weighted distribution of $C_T$ and Figure (b) shows the weighted distribution of $C_T$. Both distributions are fitted to equation 46 and the fit parameters and reduced $\chi^2$ are shown for each fit. 15 bins were used for each plot. The grey lines indicate the $1\sigma$ tolerance of the actual fit, shown in red.

parameters are used to produce the grey fits shown in figure 25. From the integrals, the uncertainties in $A_T$ are calculated through error propagation. The issue occurs when considering the yield for the constraints on $C_T$. A distribution is subject to the binning scheme used and in particular, $C_T$ is used to calculate the number of particle for the given constraint. Hence adjusting the bin numbers might adjust the contraint of the asymmetries so the yield being defined as the integral of $C_T$ is insufficient. An alternate approach is to define the yield through fitting a different parameter. The most obvious choice is to fit the centre of mass energy of the respective decays i.e. $m_{B^0}$ and $m_{\bar{B}^0}$, and so the distribution is not correlated to the $C_T$ constraints directly. Hence calculate the yield of the data for each contraint, where the yield $\eta$ and the yield of the conjugate decay $\bar{\eta}$ are defined as:

$$\eta = \int_{-\infty}^{\infty} f(m_{B^0}) dm_{B^0}, \tag{47}$$

$$\bar{\eta} = \int_{-\infty}^{\infty} f(m_{\bar{B}^0}) dm_{\bar{B}^0}, \tag{48}$$

Here, $f$ is the Gaussian function previously fitted. Though a Breit Wigner curve would be more accurate, for the given sample size equation 46 will suffice and, The integral itself is definite so can be calculated easily whereas, the Breit Wigner curve cannot. By using the substitution $u = \frac{x-B}{\sqrt{2}C}$ into equation 46 one can show:

$$\int_{-\infty}^{\infty} f(x) dx = \sqrt{2\pi} AC. \tag{49}$$

Therefore, the uncertainty in the yield is simply the quadrature sum of the uncertainties in $A$ and $C$ for the given fit. $A_T$ is defined as

$$A_T = \frac{\eta(C_T > 0) - \eta(C_T < 0)}{\eta(C_T > 0) + \eta(C_T < 0)} \tag{50}$$

and the conjugate asymmetry is:

$$\bar{A}_T = \frac{\bar{\eta}(-\bar{C}_T > 0) - \bar{\eta}(-\bar{C}_T < 0)}{\bar{\eta}(-\bar{C}_T > 0) + \bar{\eta}(-\bar{C}_T < 0)} \tag{51}$$

As for the uncertainty of the yields, there are two distinct types of uncertainty, one which is the uncertainty that the Gaussian model correctly describes the distribution and the other is the uncertainty in the yield itself. The uncertainty in the yield is the square root of the yield. This is because the yield is effectively counting the number of events so for Gaussian distributions with sample sizes greater than 20, a Poisson approximation can be taken. The fit uncertainty indicates how well a Gaussian distribution fits the model. This is simply calculated from the error propagation of the yield defined in equation 49. Since the fits are done to histograms, the integral in equation 49 is the total frequency of the distributions thus to the get the weighted number i.e. yield, the frequency must be divided by the bin width (remember $frequency = bin\ width \times bin\ height$). Thus, the yield calculated from binned data is:

$$\eta = \frac{\sqrt{2\pi}AC}{\Delta m_{B^0}} \tag{52}$$

$$\bar{\eta} = \frac{\sqrt{2\pi}AC}{\Delta m_{\bar{B}^0}} \tag{53}$$

where, A and C are defined by equation 49 and $\Delta m_{B^0}$ is the bin width (same for $\bar{\eta}$). The fit uncertainty is

$$\sigma_f = \sqrt{\left(\frac{\sigma_A}{A}\right)^2 + \left(\frac{\sigma_C}{C}\right)^2} \tag{54}$$

for $\sigma_A$ and $\sigma_C$ being the uncertainty in the fit parameters $A$ and $C$ respectively.

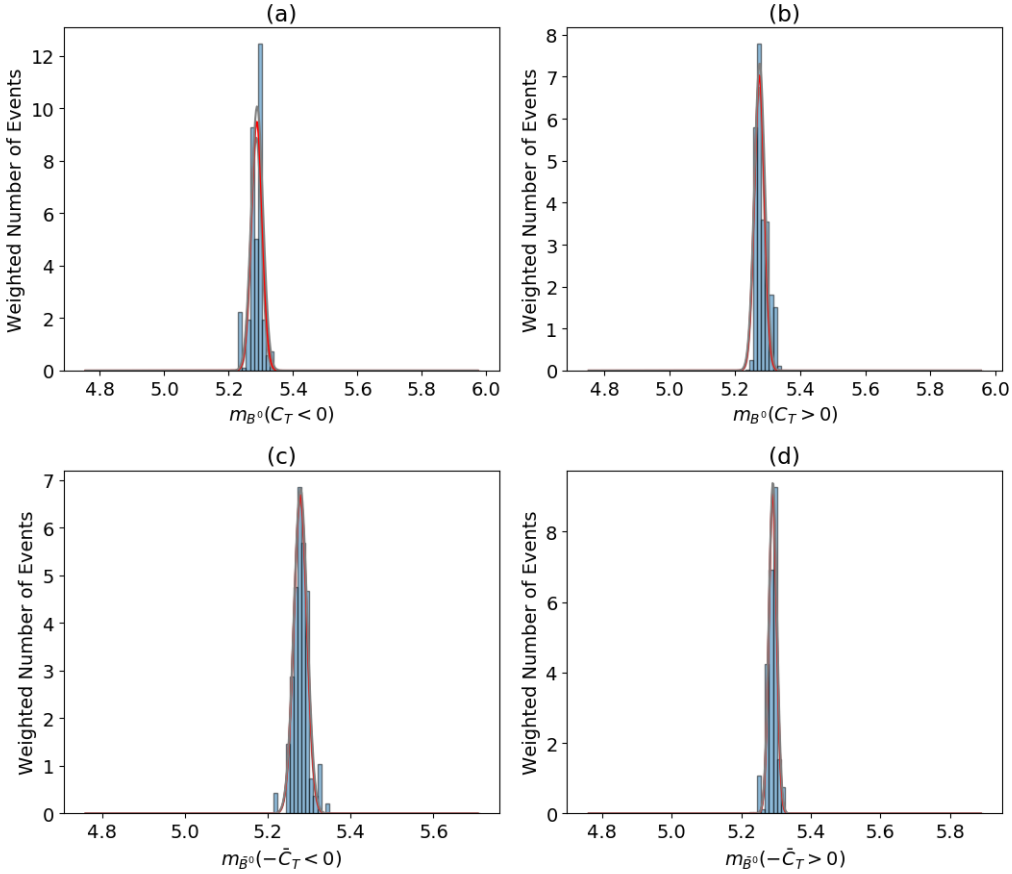


Figure 26: Plots (a) and (b) the yields for the various $C_T$ conditions and fitted distributions. Plots (c) and (d) shows the same but for the C conjugate decays. The red line indicates the best fit lines and the grey lines are the $1\sigma$ limits of the Gaussian fit. Number of events are around 600-700 for each plot and bin number used is 100 for each plot.

| plot | A | B(GeV) | C(GeV) | $\eta/\bar{\eta}$ | $\sigma_\eta/\sigma_{\bar{\eta}}$ | $\sigma_f$ |
|---|---|---|---|---|---|---|
| (a) | $9.5 \pm 0.6$ | $5.287 \pm 0.001$ | $0.017 \pm 0.001$ | 33.33 | 5.77 | 3.19 |
| (b) | $7.0 \pm 0.3$ | $5.2755 \pm 0.0008$ | $0.0156 \pm 0.0008$ | 22.62 | 4.76 | 1.45 |
| (c) | $6.7 \pm 0.1$ | $5.2784 \pm 0.0004$ | $0.016 \pm 0.0004$ | 28.09 | 5.30 | 0.85 |
| (d) | $9.1 \pm 0.3$ | $5.2905 \pm 0.0004$ | $0.0114 \pm 0.0004$ | 22.95 | 4.79 | 1.00 |

Figure 27: Shows the fit parameters and error in the yield due to the fit for each plot in figure 26. $\eta$ corresponds to plots (a) and (b) and $\bar{\eta}$ corresponds to (c) and (d).

| $A_T$ | $\bar{A}_T$ | $\mathcal{A}_{CP}$ |
|---|---|---|
| $-0.19 \pm 0.13$ | $-0.1 \pm 0.14$ | $-0.045 \pm 0.095$ |

Figure 28: Shows the parity and CP asymmetries for the run I sample calculated from the yields in figure 27.

Looking at figure 26 the resonances are narrow, and referring to figure 27 the values of $\sigma_f$ are small relative to the yield, with the largest percentage uncertainty being 9.95% so, a Gaussian function models the invariant mass distribution sufficiently. Large $\sigma_f$ values would indicate the Gaussian model is insufficient to describe the mass distributions. The least contrained fits are the amplitudes of the Gaussian where B and C are quite accurate and represent the mean mass and lifetimes of the $B^0$ and $\bar{B}^0$. From figure 26 the $1\sigma$ fit lines remain close to the best fit line, with figure 26 (a) having the largest tolerance.

Looking at figure 27, the asymmetries are all consistent with zero, which agrees with the monte carlo simulations of the decay for event number in the same order of magnitude. The magnitude of the parity violation is larger on average though, this may be due to fluctuations and so a larger sample size may result in a smaller parity asymmetry.

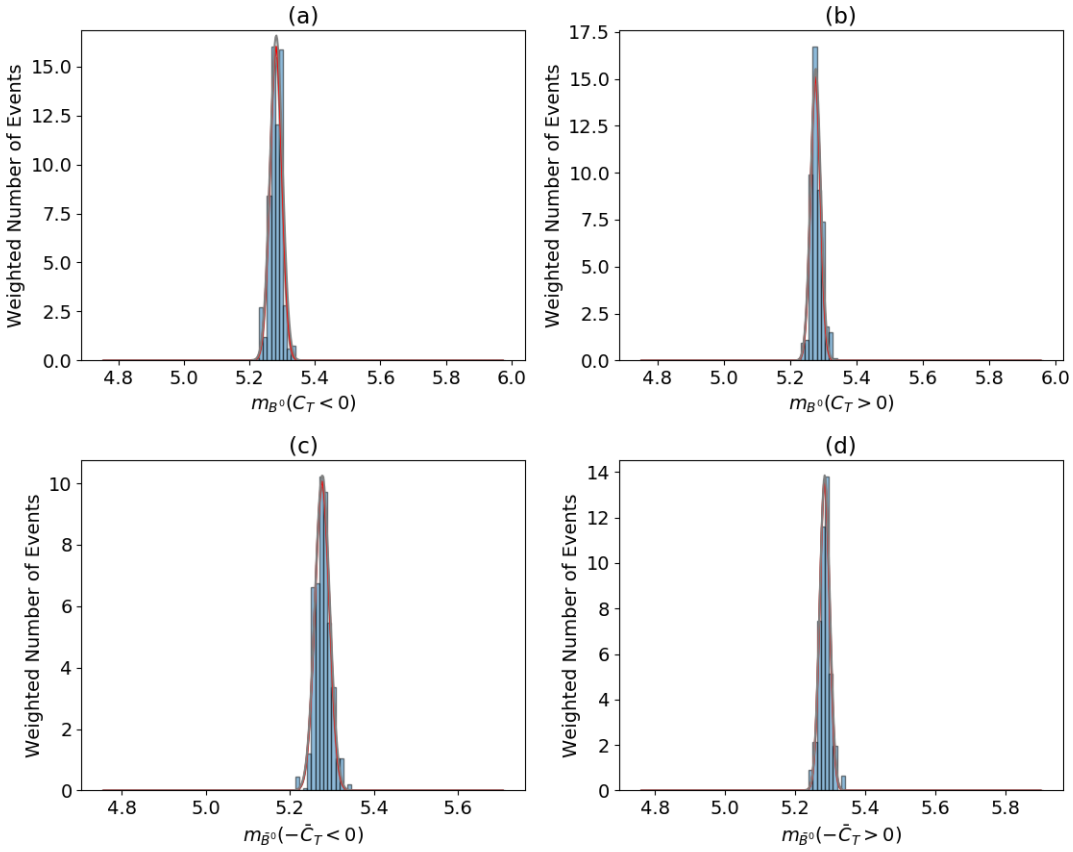


Figure 29: Plots are the same as in figure 26 but also include events from both run I and part of run II (2016) of LHCb. Number of events are around 1200 for each plot and bin number used is 100 for each plot.

| Plot | A(GeV) | B(GeV) | C | $\eta/\bar{\eta}$ | $\sigma_\eta/\sigma_{\bar{\eta}}$ | $\sigma_f$ |
|---|---|---|---|---|---|---|
| (a) | $16.0 \pm 0.6$ | $5.2813 \pm 0.0007$ | $0.0185 \pm 0.0007$ | 60.38 | 7.77 | 3.18 |
| (b) | $15.1 \pm 0.4$ | $5.2765 \pm 0.0005$ | $0.0149 \pm 0.0005$ | 46.63 | 6.83 | 1.97 |
| (c) | $10.1 \pm 0.2$ | $5.2768 \pm 0.0004$ | $0.0174 \pm 0.0004$ | 45.78 | 6.77 | 1.37 |
| (d) | $13.7 \pm 0.2$ | $5.2845 \pm 0.0002$ | $0.0143 \pm 0.0002$ | 42.56 | 6.52 | 0.98 |

Figure 30: Shows the fit parameters and error in the yield due to the fit for each plot in figure 29. $\eta$ corresponds to plots (a) and (b) and $\bar{\eta}$ corresponds to (c) and (d).

| $A_T$ | $\bar{A}_T$ | $\mathcal{A}_{CP}$ |
|---|---|---|
| $-0.13 \pm 0.10$ | $-0.04 \pm 0.10$ | $-0.046 \pm 0.072$ |

Figure 31: Shows the parity and CP asymmetries for the run II sample calculated from the yields in figure 30.

This method works but it may not produce the correct uncertainties because the data has been weighted, and is done so by fitting a model to the data. Hence fitting the resonance curve again reduces the accuracy of the yield measurement. Rather, the yield can be calculated by summing the weights for the different conditions of $C_T$ i.e. for some weight values $w_i$, the yield is:

$$\eta = \sum_{i=0}^{N} w_i \tag{55}$$

and this applied for all the $C_T$ conditions.

| $A_T$ | $\bar{A}_T$ | $\mathcal{A}_{CP}$ |
|---|---|---|
| $-0.11 \pm 0.095$ | $-0.027 \pm 0.105$ | $-0.068 \pm 0.071$ |

Figure 32: Shows the calculated asymmetries for LHCb data by calculating the yields as shown in equation 55.

The difference in figures 31 and 30 are that the mean values of the parity asymmetries decrease and the CP asymmetry increase though the uncertainties remain the same. Hence for this sample size the analysis could be done in either way with minimal effect but if the sample size increased and the trends observed between the two remain, then parity violation may be predicted at an excess if the integral method is used.

The ideal scenario would be to split the data for the various conditions of $C_T$ and $-\bar{C}_T$ and *then* weight the data and calculate the yield from equation 55. A crude attempt of this would require a cut of the data near the resonance of the B mesons and then repeat the analysis used for the monte carlo simulated data i.e. ignore the noise. From figure 29 an appropriate region to cut the data is between 5.2GeV and 5.4GeV, as shown in figure 33.

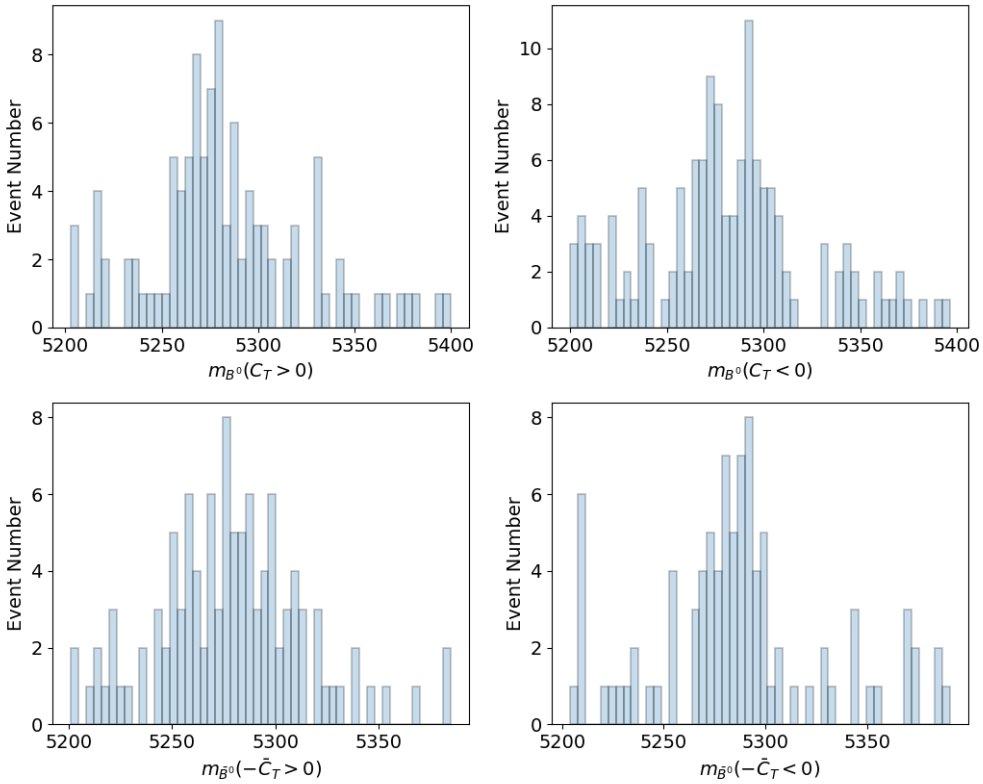


Figure 33: Plots are the distributions of the invariant masses of the $B^0$ and $\bar{B^0}$ of the same LHCb data used previously. The data is cut near the centre of the B meson resonances.

| $A_T$ | $\bar{A}_T$ | $\mathcal{A}_{CP}$ |
|---|---|---|
| $-0.128 \pm 0.064$ | $-0.085 \pm 0.07$ | $-0.021 \pm 0.047$ |

Figure 34: Shows results of the asymmetries by counting the event numbers near the resonances and making the assumption the noise near the resonance is low.

Looking at figure 34 it is clear by assuming that the noise near the B0 resonance is negligible, the mean values of the asymmetries are representative of the method used to produce figure 30, whereas the uncertainties drop significantly compared to when the data was weighted. This shows that the number of $B^0$ and $\bar{B^0}$ decays are being overestimated, as the parity asymmetries are more statistically significant than when considering the weighted data.

**More Data:**

Sample now contains both trigger on signal (what we used before) and trigger independent of signal, with the following efficiencies:

| | |
|---|---|
| Run1(TOS) | 0.9968 |
| Run1(TIS) | 0.9988 |
| Run2(TOS) | 0.9693 |
| Run2(TIS) | 0.9708 |

Figure 35: Shows the global efficiency of the samples for each run and signal dependance. Run2 only corresponds to the year 2016.

Results of the asymmetries are as follows:

| $A_T$ | $\bar{A}_T$ | $\mathcal{A}_{CP}$ |
|---|---|---|
| $-0.14 \pm 0.068$ | $0.004 \pm 0.074$ | $-0.072 \pm 0.05$ |

Figure 36: Shows the calculated asymmetries for LHCb data for files shown in figure 35.

Compared to figure 32, the value of $A_T$ appears to converge to a non zero value, but still, is not statistically significant. $\bar{A}_T$ appears to converge to a zero value and due to this $A_{CP}$ converges to a non-zero value (not statistically significant). Note that the TIS included data increases the yield from around 200 to 400, though the actual number of events increases by around 100 so it seems the TIS data has less background in the total signal. Note for these new event files, there are 1025 total unweighted events.

## 2.8 Binned MC data

Similar to the KKPiPi analysis, the phase space can be binned through the 5 CM variables and so the asymmetries can be calculated per region of phase space. The binning scheme used varies the region limits such that two conditions are met; the number of events in each phase space region is equal (ore close to equal) and that the total event number is conserved up to a tolerance. This algorithm results in loss of data by attempting to satisfy the first condition hence, the second condition is required. Once the events are binned, the triple product quantity can be calculated and P and CP asymmetries are calculated in the usual way for the MC data.

Referring to figure 38, every bin is cut in the middle of the extreme values as expected, except for $m_{cd}$, which is actually cut near the $K*$ resonance peak as this peak is very distinct. The reason $m_{ab}$ was not cut in such a way is because the distribution consists of many prominent resonances across the entire mass range, hence compared to $m_{ab}$ is fairly uniform.

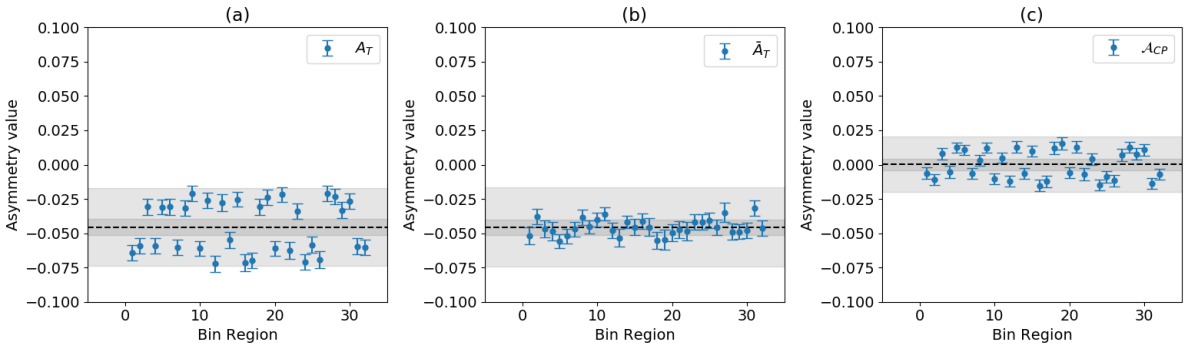


Figure 37: Shows the various asymmetries calculated for each region of phase space. The black line indicate the mean value (entire phase space considered) and the grey and light grey regions represent the $1\sigma$ and $5\sigma$ uncertainty regions of the overall asymmetries. Bin regions are defined in figure 38. The number of events used was $10^6$ for both regular and conjugate events.

From figure 37 the values of the asymmetries in each bin fluctuate above and below the mean value, in particular, figure 37 a shows that there is significant offsets in the asymmetries per region than compared to 37 b. This is likely to be an artefact of the binning scheme since binning was optimised with respect to the regular decays. This would occur since $\phi$ is itself a triple product asymmetry and so is a parity sensitive quantity similar to $C_T$, so the binning of $\phi$ heavily distinguishes parity asymmetries in each region. Note that the order in which the parameters were binned was attempted to eliminate this artefact but made no difference. Note the order chosen in figure 38 was done as to provide the most evenly distributed events per phase space region. More cuts could have been made in the phase space but the number of bins goes up by $(number\ of\ cuts)^5$ so if an additional cut was used, there would be 243 different regions and the event numbers in each would be too low, resulting in larger uncertainties shown in figure 37.

| Region | $\cos(\theta_a)$ | $\cos(\theta_c)$ | $m_{cd}(\mathrm{MeV}/c^2)$ | $m_{ab}(\mathrm{MeV}/c^2)$ | $\phi$ |
|---|---|---|---|---|---|
| 1 | (0.0, 1.0) | (0.0, 1.0) | (633.25, 896.6) | (3729.77, 4053.82) | (-1.57, 0.0) |
| 2 | (0.0, 1.0) | (0.0, 1.0) | (633.25, 896.6) | (4053.82, 4377.88) | (-1.57, 0.0) |
| 3 | (-1.0, 0.0) | (0.0, 1.0) | (896.6, 1528.34) | (4053.82, 4377.88) | (-1.57, 0.0) |
| 4 | (0.0, 1.0) | (-1.0, 0.0) | (896.6, 1528.34) | (4053.82, 4377.88) | (-1.57, 0.0) |
| 5 | (-1.0, 0.0) | (0.0, 1.0) | (633.25, 896.6) | (3729.77, 4053.82) | (-1.57, 0.0) |
| 6 | (-1.0, 0.0) | (0.0, 1.0) | (896.6, 1528.34) | (3729.77, 4053.82) | (0.0, 1.57) |
| 7 | (0.0, 1.0) | (-1.0, 0.0) | (633.25, 896.6) | (3729.77, 4053.82) | (0.0, 1.57) |
| 8 | (-1.0, 0.0) | (0.0, 1.0) | (896.6, 1528.34) | (3729.77, 4053.82) | (-1.57, 0.0) |
| 9 | (-1.0, -0.0) | (-1.0, 0.0) | (896.6, 1528.34) | (3729.77, 4053.82) | (0.0, 1.57) |
| 10 | (0.0, 1.0) | (0.0, 1.0) | (896.6, 1528.34) | (3729.77, 4053.82) | (-1.57, 0.0) |
| 11 | (-1.0, 0.0) | (0.0, 1.0) | (633.25, 896.6) | (4053.82, 4377.88) | (-1.57, 0.0) |
| 12 | (0.0, 1.0) | (0.0, 1.0) | (896.6, 1528.34) | (3729.77, 4053.82) | (0.0, 1.57) |
| 13 | (-1.0, 0.0) | (0.0, 1.0) | (633.25, 896.6) | (4053.82, 4377.88) | (0.0, 1.57) |
| 14 | (0.0, 1.0) | (-1.0, 0.0) | (633.25, 896.6) | (4053.82, 4377.88) | (0.0, 1.57) |
| 15 | (-1.0, 0.0) | (-1.0, 0.0) | (633.25, 896.6) | (3729.77, 4053.82) | (-1.57, 0.0) |
| 16 | (0.0, 1.0) | (-1.0, 0.0) | (896.6, 1528.34) | (4053.82, 4377.88) | (0.0, 1.57) |
| 17 | (0.0, 1.0) | (-1.0, 0.0) | (633.25, 896.6) | (4053.82, 4377.88) | (-1.57, 0.0) |
| 18 | (-1.0, 0.0) | (0.0, 1.0) | (896.6, 1528.34) | (4053.82, 4377.88) | (0.0, 1.57) |
| 19 | (-1.0, 0.0) | (-1.0, 0.0) | (896.6, 1528.34) | (4053.82, 4377.88) | (-1.57, 0.0) |
| 20 | (0.0, 1.0) | (-1.0, 0.0) | (633.25, 896.6) | (3729.77, 4053.82) | (-1.57, 0.0) |
| 21 | (-1.0, 0.0) | (-1.0, 0.0) | (896.6, 1528.34) | (3729.77, 4053.82) | (-1.57, 0.0) |
| 22 | (0.0, 1.0) | (0.0, 1.0) | (896.6, 1528.34) | (4053.82, 4377.88) | (0.0, 1.57) |
| 23 | (-1.0, 0.0) | (-1.0, 0.0) | (633.25, 896.6) | (3729.77, 4053.82) | (0.0, 1.57) |
| 24 | (0.0, 1.0) | (0.0, 1.0) | (896.6, 1528.34) | (4053.82, 4377.88) | (-1.57, 0.0) |
| 25 | (0.0, 1.0) | (-1.0, 0.0) | (896.6, 1528.34) | (3729.77, 4053.82) | (0.0, 1.57) |
| 26 | (0.0, 1.0) | (0.0, 1.0) | (633.25, 896.6) | (4053.82, 4377.88) | (0.0, 1.57) |
| 27 | (-1.0, 0.0) | (0.0, 1.0) | (633.25, 896.6) | (3729.77, 4053.82) | (0.0, 1.57) |
| 28 | (-1.0, 0.0) | (-1.0, 0.0) | (633.25, 896.6) | (4053.82, 4377.88) | (-1.57, 0.0) |
| 29 | (-1.0, 0.0) | (-1.0, 0.0) | (896.6, 1528.34) | (4053.82, 4377.88) | (0.0, 1.57) |
| 30 | (-1.0, 0.0) | (-1.0, 0.0) | (633.25, 896.6) | (4053.82, 4377.88) | (0.0, 1.57) |
| 31 | (0.0, 1.0) | (0.0, 1.0) | (633.25, 896.6) | (3729.77, 4053.82) | (0.0, 1.57) |
| 32 | (0.0, 1.0) | (-1.0, 0.0) | (896.6, 1528.34) | (3729.77, 4053.82) | (-1.57, 0.0) |

Figure 38: Shows the regions of phase space defined by number. Note that the binning scheme was done with respects to the regular decay and then used for the conjugate decay, as to keep the bin regions consistent when calculating $\mathcal{A}_{CP}$. The generic particle names refer to equation 8 i.e. $c$ refers to $K^+$ for the regular decay and $K^-$ for the conjugate decay etc.

## 2.9 model-Fitting

Tested the single signal fitter in AMPGEN with monte carlo generated data which gives figure 39.

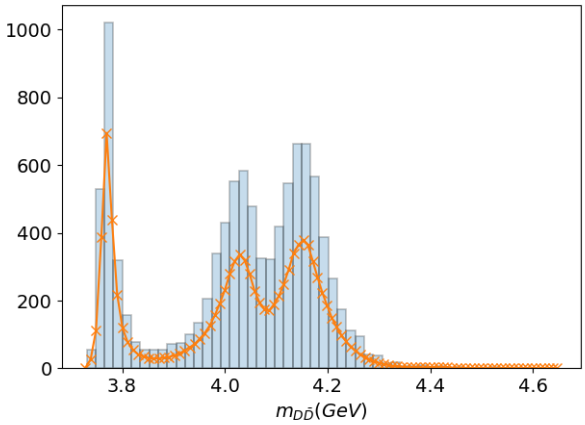


Figure 39: Shows the histogram of $m_{D\bar{D}}$ generated with AMPGEN for 10000 events and the fit produced by the signal fitter of said data (orange). There is a difference in the scale as the fitter used a different number of samples to produce the fit.

if we use the same model and fit it to the LHCb data, we get figure 40.

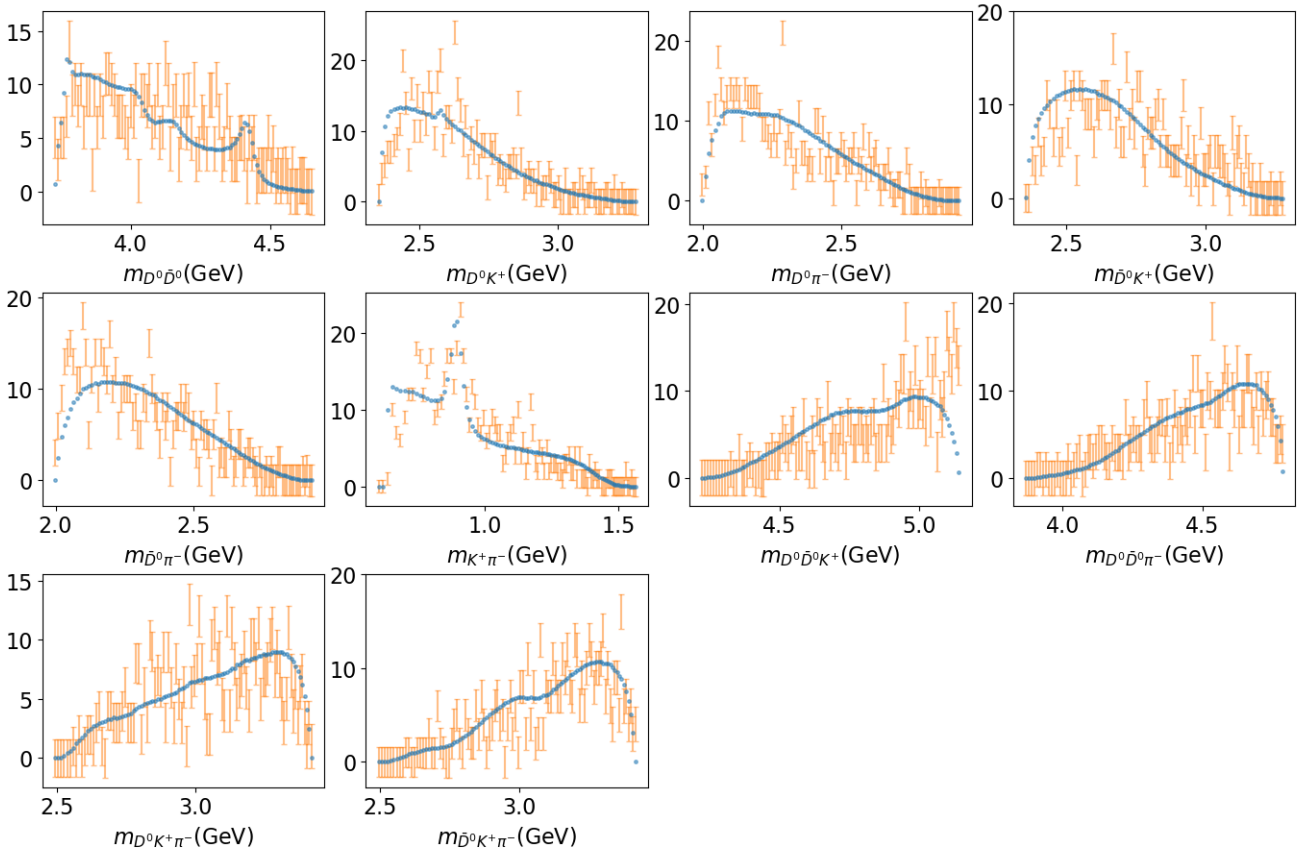


Figure 40: Shows the all the resonant masses from the LHCb sample data, with the decay model fitted. The total number of events is 551, with the weighted number being 213. The fit produced by the signal fitter is in blue. Note the histogram errors are $1\sigma$ of the square root of the sum of squares of the weights (set to 1). The Chi squared per bin is 5.182.

From the $m_{D^0\bar{D}^0}$ and $m_{K^+\pi^-}$ some resonances are visible from the fit, namely the $K^*(800)$ and the $\psi(3770)$. Other resonances though looking prominent in the fit is not very clear in the data such as the $\psi(4415)$ and $\psi(4160)$ for the $m_{D^0\bar{D}^0}$ projection and $D^*_{s2}(2573)$ in projection $m_{D^0K^+}$. As the sample size cant be increased, resonances which have a poor fit fraction can be eliminated from the model to see if the projections are improved. As a definition a poor fit fraction will be one with errors less than 3 sigma.

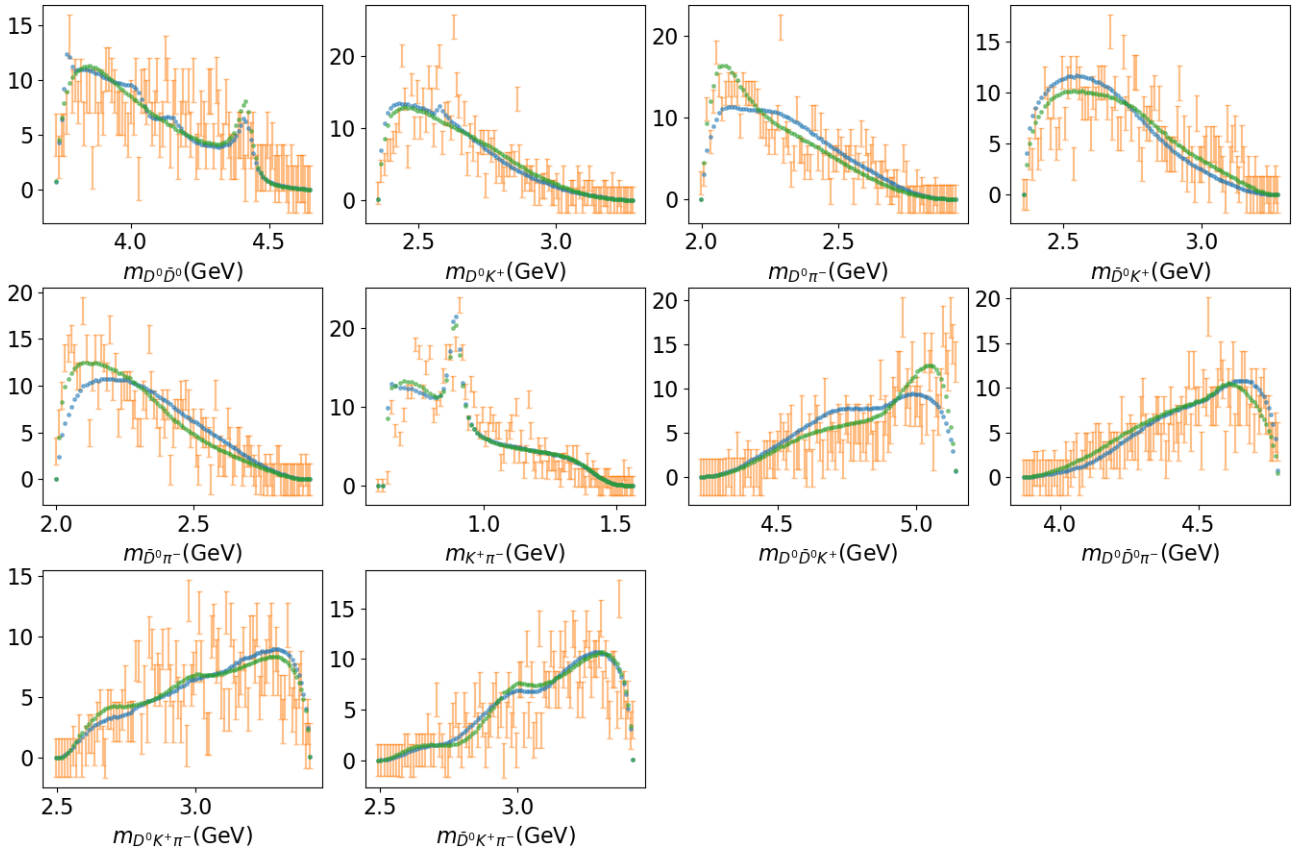


Figure 41: Shows the projections from figure 40 with the model with removed resonances as well (in green). The Chi squared per bin is 5.3540 for the green fit lines.

The removal of the poor fit fractions makes some resonances more apparent in the fit such as the $\psi(4415)$ and resonances which are removed are clear by studying the two different projections in figure 41.

| Decay Amplitude | Fit Fraction |
|---|---|
| B0{NonResS0{D0,Dbar0},K(0)*(1430)0{K+,pi-}} | $0.32 \pm 0.03$ |
| B0{psi(4415)0{D0,Dbar0},K(0)*(1430)0{K+,pi-}} | $0.2 \pm 0.02$ |
| B0{K(0)*(800)0{K+,pi-},NonResS0{D0,Dbar0}} | $0.08 \pm 0.02$ |
| B0{NonResS0{D0,Dbar0},K*(892)0{K+,pi-}} | $0.07 \pm 0.02$ |
| B0[D]{psi(4415)0{D0,Dbar0},K*(892)0{K+,pi-}} | $0.06 \pm 0.02$ |
| B0[P]{psi(4415)0{D0,Dbar0},K*(892)0{K+,pi-}} | $0.04 \pm 0.01$ |
| B0[S]{psi(4160)0{D0,Dbar0},K*(892)0{K+,pi-}} | $0.02 \pm 0.01$ |
| B0[P]{psi(3770)0{D0,Dbar0},K*(892)0{K+,pi-}} | $0.02 \pm 0.01$ |
| B0[D]{psi(4040)0{D0,Dbar0},K*(892)0{K+,pi-}} | $0.01 \pm 0.01$ |
| B0[S]{psi(4040)0{D0,Dbar0},K*(892)0{K+,pi-}} | $0.01 \pm 0.01$ |
| B0[P]{psi(4040)0{D0,Dbar0},K*(892)0{K+,pi-}} | $0.009 \pm 0.006$ |
| B0{psi(4040)0{D0,Dbar0},K(0)*(800)0{K+,pi-}} | $0.008 \pm 0.005$ |
| B0[S]{psi(3770)0{D0,Dbar0},K*(892)0{K+,pi-}} | $0.005 \pm 0.001$ |
| B0{D(s2)(2573)+{D0,K+},Dbar0,pi-} | $0.005 \pm 0.003$ |
| B0[D]{psi(4160)0{D0,Dbar0},K*(892)0{K+,pi-}} | $0.004 \pm 0.005$ |
| B0{psi(4160)0{D0,Dbar0},K(0)*(800)0{K+,pi-}} | $0.004 \pm 0.005$ |
| B0{psi(4415)0{D0,Dbar0},K(0)*(800)0{K+,pi-}} | $0.004 \pm 0.005$ |
| B0{psi(4160)0{D0,Dbar0},K(0)*(1430)0{K+,pi-}} | $0.003 \pm 0.004$ |
| B0[S]{psi(4415)0{D0,Dbar0},K*(892)0{K+,pi-}} | $0.003 \pm 0.002$ |
| B0{psi(4040)0{D0,Dbar0},K(0)*(1430)0{K+,pi-}} | $(1 \pm 9) \times 10^{-4}$ |
| B0{psi(3770)0{D0,Dbar0},K(0)*(800)0{K+,pi-}} | $(0.7 \pm 7.1) \times 10^{-4}$ |
| B0[P]{psi(4160)0{D0,Dbar0},K*(892)0{K+,pi-}} | $(0.08 \pm 1.57) \times 10^{-4}$ |
| B0[D]{psi(3770)0{D0,Dbar0},K*(892)0{K+,pi-}} | $(0.3 \pm 9.5) \times 10^{-5}$ |
| B0{psi(3770)0{D0,Dbar0},K(0)*(1430)0{K+,pi-}} | $(0.2 \pm 6.6) \times 10^{-5}$ |
| Total fit fraction | $0.87 \pm 0.04$ |

Figure 42: Shows the Decay amplitudes as written in the event file and the fit fractions caclulated from the signal only fitter in AmpGen (Note the total fit fraction doesn't need to be 1).

| Decay Amplitude | Fit Fraction |
|---|---|
| B0{NonResS0{D0,Dbar0},K(0)*(1430)0{K+,pi-}} | $0.34 \pm 0.07$ |
| B0{psi(4415)0{D0,Dbar0},K(0)*(1430)0{K+,pi-}} | $0.20 \pm 0.09$ |
| B0{NonResS0{D0,Dbar0},K*(892)0{K+,pi-}} | $0.09 \pm 0.02$ |
| B0{K(0)*(800)0{K+,pi-},NonResS0{D0,Dbar0}} | $0.09 \pm 0.03$ |
| B0[P]{psi(4415)0{D0,Dbar0},K*(892)0{K+,pi-}} | $0.04 \pm 0.01$ |
| B0[D]{psi(4415)0{D0,Dbar0},K*(892)0{K+,pi-}} | $0.3 \pm 0.01$ |
| B0[S]{psi(3770)0{D0,Dbar0},K*(892)0{K+,pi-}} | $(4 \pm 8) \times 10^{-4}$ |
| Total fit fraction | $0.7 \pm 0.2$ |

Figure 43: Shows the Decay amplitudes for resonances with poor fit fractions removed in figure 42 as written in the event file and the fit fractions calculated from the signal only fitter in AMPGEN.

Checklist:
• Catch up ✓
• Try AmpGen on bayban (struggling with issues regarding Minuit2) ✓
• Make sure all code is ready i.e. can you calculate dalitz plot parameters and plots etc. ✓
• Try to construct AmpGen event file for the decay. ✓
• test for p violation in $D \to K^+K^-\pi^+\pi^-$ from AmpGen ✓
• test CP violation for $D \to K^+K^-\pi^+\pi^-$ by flipping signs of 3-momenta of events already made (check with literature) ✓
• same for B decay ✓
• add NonRes optimisation ✓
• split spins of B decays into s p d channels (divide amplitudes evenly) and compare results ✓
• adjust P waves and check P violation. ✓
• try real sample (figure out how noise was reduced for final report)
• Try to implement awesome sensitivity plots ✓
• Upload (pdf at least) somewhere paras and jonas can see it (github?) ✓
• find maximal p violation conditions. ✓
• study sp waves for 1 resonance ✓
• study sp waves for massive relative amplitudes (100-10000) ✓
• study sp waves for varying seeds (removes any bias from random number generator) ✓
• study sp waves and CP violation ✓
• try model fitter for AMPGEN ✓
• model fit real data to our model (with or without efficiency).
• (extra) try binning by density ✓
• Fit $C_T$ for real data, integrate $C_T > 0$ and $C_T < 0$ to find $A_T$ ✓

# References


[1] M. Gronau and J. L. Rosner, "Triple-product asymmetries in K, $D_{(s)}$, and $B_{(s)}$ decays," *Physical Review D*, vol. 84, nov 2011.

[2] Y. Nagashima, *Elementary Particle Physics*. Wiley-VCH Verlag GmbH & Co. KGaA, aug 2010.

[3] R. A. et. al., "Search for CP violation using $T-$odd correlations in $D_0 \to K^+K^+\pi^+\pi^-$ decays," *Journal of High Energy Physics*, vol. 2014, oct 2014.